Co-activation Pattern Analysis of Brain fMRI Signal at Avalanches

By

Junlin Guo

Thesis

Submitted to the Faculty of the

Graduate School of Vanderbilt University

in partial fulfillment of the requirements

for the degree of

MASTER OF SCIENCE

in

ELECTRICAL ENGINEERING

June 30, 2020

Nashville, Tennessee

Approved:

D. Mitchell Wilkes, Ph.D.

Zhaohua Ding, Ph.D.

To my parents

and

To my siblings.

ACKNOWLEDGEMENTS

I would first like to express the deepest gratitude to my advisor, Dr. Mitch Wilkes, who has convincingly guided me to be professional. Without his persistent mentoring in research and writing, the thesis would not have been completed. I would also like to thank Drs. Zhaohua Ding, Catie Chang, for providing suggestions to this work.

I would also express my sincere appreciation to Dr. Alan Peters, who has helped me during the two-year master's program. I would like to thank my lab mate Nazirah Mohd Khairi for teaching me how to deal with the dataset and all her invaluable assistance. Lastly, I wish to show my gratitude to my friends Haley Blankenship, for all her support in proofreading and insightful writing instructions, Chelsea Janda, and Shengchao Zhang, who have consistently supported me in the completion of the thesis.

TABLE OF CONTENTS

LIST OF TABLES

LIST OF FIGURES

CHAPTER 1

INTRODUCTION

The human brain, in health and disease, is a large, complex information processing system [1]. It has always been of overwhelming interest for researchers to understand the functions of the brain, which is concentrated on the analysis of large-scale spatiotemporal patterns of brain activity [2]-[7]. Studies have shown that some information propagation in the brain is organized as spatiotemporal cascades of any size and length, termed "neuronal avalanches," underlying a critical branching process [8]-[12]. The propagation of cascades (avalanches) is also claimed to be an organizing principle for neuronal activity [13], [14].

The advent of novel functional magnetic resonance imaging (fMRI) modality provided new opportunities to study the brain. fMRI scans at rest, for instance, significantly improve the understanding of the brain organization by observing the manifestation of spontaneous neuronal activity [5]. Besides, fMRI also assists in studying mental illness and brain disorder. [15]-[20] show how fMRI analysis is involved in studying the progression of Alzheimer's disease (AD).

Similarly, given the continuous improvement in spatial and temporal resolutions of brain imaging, there has been an increased interest in exploring the avalanches via fMRI data. Tagliazucchi [21] proposes an approach of detecting avalanches of resting-state fMRI (rsfMRI) data via a novel point process technique. In Tagliazucchi's work, avalanches are encoded in time as a series of suprathreshold crossings of the blood-oxygen-level-dependent (BOLD) signal at a seed region. It is also important to note that utilizing these extracted points can produce resting-state activation maps comparable to utilizing the full BOLD signal. This work, for the first time, provides a seed-based scheme to detect avalanches with rsfMRI, which indicates a possibility of substantially reducing the dataset when

exploring large-scale brain activity. This seed-based scheme has been extensively investigated by researchers and applied to brain analysis [22]-[24].

However, the global fMRI signal fluctuations have also shown a correlation with the brain-wide activity [25]. Studies have demonstrated that the rsfMRI connectivity is associated with the global fMRI signal, where the covariation of brain activity can be condensed into brief epochs [26]-[28]. An intuitive and thought-provoking question would be whether it is possible to detect avalanches from the global fMRI signal calculation. The publication from Tagliazucchi [21] implies an approach by tracing the *largest* size of activated elements (i.e., clusters of voxels) throughout the brain over time. Avalanches in the global signal then correspond to the periods when clusters of a vast number of activated voxels exist on the cortex. Fueled by this newfound approach from Tagliazucchi, Bell [29] proposes an instantaneous whole-brain correlation (IWBC) analysis that produces a time course of overall correlation in the brain, and accordingly, employs it as a tool to define avalanches. This work shows that, in contrast to non-avalanching periods, brain activity is dominated by IWBC avalanches, where the brain co-activation patterns (CAPs) have more connections.

Thus, Bell [29] and Tagliazucchi [21] are the primary referring sources of the thesis. This thesis attempts to explore the brain CAPs at IWBC avalanches. In this work, each time point in IWBC assigns a brain CAP, and the Markov Model (MM) [30] is then utilized to understand the CAP dynamics. This allows visible CAP transitions and a probabilistic interpretation of the consistency of CAPs. Additionally, this work presents the spatial CAPs in IWBC, which can provide insights into identifying the synchronization throughout the brain. Furthermore, the few gigantic IWBC avalanche peaks are investigated and shown to compress the covariation of CAP in the entire series. In summary, the thesis extends the work from Tagliazucchi [21] and Bell [29] by performing CAP analysis throughout the brain based on the novel tool IWBC.

The remainder of this thesis is composed of four themed chapters. These separated chapters, coupled with the introduction, outline the fundamental structure of this work. Chapter 2 provides the background,

which introduces the fMRI modality and schemes of defining avalanches. The following chapter 3 is concerned with the methodology used for the thesis, including undertaking the procedure and analysis approach. Chapter 4 analyzes the results for the thesis. Finally, in chapter 5, the thesis closes with a summary of the entire work and speculation on future directions.

CHAPTER 2

BACKGROUND

This chapter provides the background for the thesis. It begins with the fundamental basics of the novel modality, functional magnetic resonance imaging (fMRI). The following 2.2 introduces the resting-state fMRI (rsfMRI), which this work analyzes. Lastly, 2.3 elucidates the background of "avalanche," including how it has been defined and investigated.

2.1 Basics of fMRI

Recently, magnetic resonance imaging (MRI) has been used and widely accepted in studying the brain. This neuroimaging technique employs the conventional magnetic resonance method to obtain structural and anatomical information about the brain. The related modality structural MRI (sMRI), for instance, provides a detailed 3D volumetric and voxel-based brain morphology. Apart from providing brain anatomical information, the MRI also extends to perform regional brain activity analysis. The novel functional MRI (fMRI) modality delineates the real-time maps of blood oxygenation (metabolic demands) in the brain underlying physiological conditions [31]. The fMRI then constructs a 3D volume series at relatively high temporal and spatial resolutions, which potentially enables a clear interpretation of brain activity [29]. The following will present the gist of the fMRI physics and physiology summarized from [29]-[32].

2.1.1 fMRI physics

The essence of the MRI technique is the use of static and variable magnetic fields to perturb hydrogen atoms within the tissue and measuring the resultant magnetic resonance by receiver coils. For

MRI scanners, common strengths of static magnetic fields are 1.5 Tesla (T), 3, 4, and 7T, which are at least 30K times the Earth's magnetic field (5E-5T) [33]. The following summarizes the principle of MRI signal acquisition given such a strong external magnetic field.

Precession initiation in a spin system

When placed in a strong external static field denoted as B_0, provided by an MRI scanner, the protons will initiate precession that is parallel to B_0 at a frequency known as Larmor frequency [34], which is based on the strength of B_0 and characteristic of the tissue. The protons correspond to hydron protons due to the predominant concentration of water molecules and fats within the tissue. The initiation then leads to an equilibrium state (the low energy state) for this spin system, in that the net magnetization (M) aligns along with B_0. However, it is difficult to detect the M by the receiver coil (antenna) underlying the B_0 alignment. Thus, the radio frequency (RF) excitation pulse is introduced to move the precession away from the axis of B_0 in order to detect M [35].

Magnetic resonance (MR) collection

Figure 2.1, presented in [29], [36], illustrates the key aspects of an MR measure. Figure 2.1A, B, C show the excitation and relaxation steps required for MRI signal generation. Figure 2.1A represents the equilibrium state with M aligning along with the B_0 (longitudinal axis). In Figure 2.1B, the introduction of a 90° excitation Larmor RF pulse causes the M to tip into the transverse plane (the high energy state). The key of the MR measure is to measure the relaxation time of M moving back to the low energy state after removing the RF pulse. Given Figure 2.1B, ideally, the longitudinal component of M recovers from zero after the distortion. This longitudinal measurement then generates the T1 recover or T1 signal that can be measured by receiver coils. Similarly, by measuring the transverse component of M after the distortion, the T2 decay or T2 signal can be measured. Accordingly, the T1 or T2 signal is utilized and collected for sMRI, in that biological matter differs on T1, T2 relaxation time depending on its composition.

Figure 2.1C, D show the local variations of M in the transverse plane. This incoherence in the spin system is due to the inhomogeneity of the local magnetic field. Figure 2.1 E, F, and G then show the 180° refocusing RF pulse for reversing the incoherence. Figure 2.2 overall demonstrates using an entire spin-echo pulse sequence for MRI signal acquisition. Details regarding this spin-echo pulse sequence demonstration and other types of RF pulse sequence, such as gradient-echo, magnetization-prepared rapid gradient echo (MPRAGE), and echo-planar (EPI) imaging, can be found in [29], [32], [37].

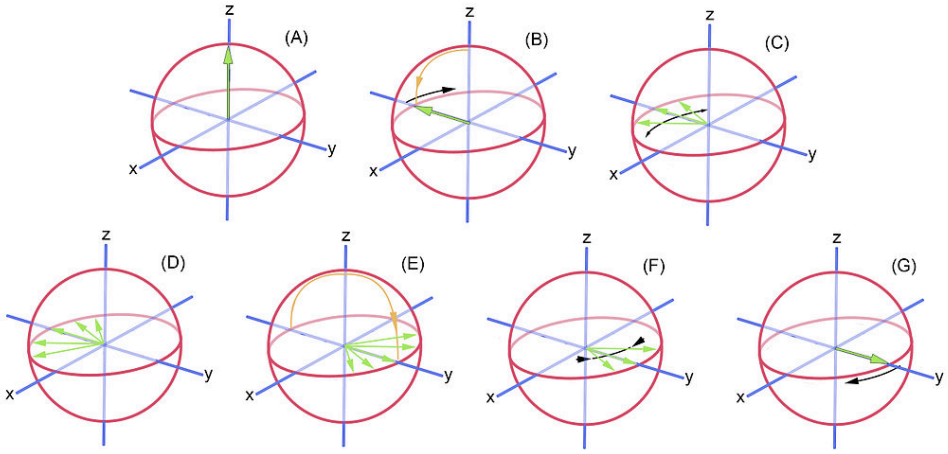

Figure 2.1 MR collection via spin echo pulse sequence [36]

MR spatial encoding and image construction

As shown in Figure 2.1, the distortion of M is through manipulating the magnetic field gradient along the z-axis, G_z. Consequently, combined with Larmor RF pulse, slices in the x-y plane are selectively excited. Similarly, the other two linear magnetic field gradients (i.e., G_x and G_y, respectively) can also play out during slicing [38]. Thus, these three orthogonal linear magnetic field gradients enable MR its three-dimensional capability and spatial specificity, known as spatial encoding. In conclusion, the combination of MRI gradient coils and RF pulse sequence allows for imaging any voxel in the brain. The resultant image, sMRI, for instance, is a 3D T1 or T2 contrast image.

2.1.2 fMRI physiology

The fMRI is a refined MRI method, and accordingly, shares the same principle of MRI signal acquisition. The difference relies on the signal measured in fMRI, which is the blood-oxygen-level-dependent (BOLD) signal, and it reflects the oxygen consumption of active neurons. It is also important to note that the varying BOLD signal values are due to brain activity [31]. Therefore, fMRI is not a direct measure of neural activity but instead measures the consequence of the neural activity.

In fMRI scanning, the BOLD signal is associated with the T2* signal, which represents the homogeneity of the local magnetic field. The field inhomogeneity (shown as the spin system incoherence in Figure 2.1C, D) induces a reduction in the BOLD signal. According to the difference in magnetic quality, oxygenated and deoxygenated blood are diamagnetic and paramagnetic, respectively [31].

An increase in local brain activity will cause a regional influx of diamagnetic oxygenated blood, which increases the local field homogeneity. Thus, an increase in the BOLD signal can be captured in that region. Decreased activity, on the other hand, corresponds to a regional trend of deoxygenated blood, and thus, reduces the BOLD signal. Additionally, the Hemodynamic response function (HRF) [39] represents the characteristic BOLD signal response triggered by neural activity, which further approves the BOLD fMRI mechanism.

2.2 Resting-state fMRI (rsfMRI) analysis

As stated in [40], this novel modality that employs BOLD signal measures is typically applied to task-based fMRI (tfMRI) data. The rsfMRI scans, however, measure the low frequency (<0.1 Hz) spontaneous fluctuations in BOLD signal when the subject is not engaged in any explicit task [29], [40]. Many studies have shown that analysis of the brain in the rsfMRI effectively reveals the functional architecture of the brain [40]-[42]. Through applying rsfMRI, spatially disparate areas that display synchronous BOLD fluctuations at rest can be identified, which is appropriately termed as functional connectivity (FC) [42]-[44]. The identification results in some networks with consistently high

internetwork connectivity [29], known as resting-state networks (RSNs). RSNs are thought to represent the intrinsic brain connectivity, and accordingly, involved in many rsfMRI studies as well as task-based designs [45]-[49]. Moreover, studies also hypothesize the presence of two opposing RSN systems in the brain, which are "task-negative" and "task-positive" RSNs, respectively [50]-[52]. Similar terms also refer to "intrinsic" and "extrinsic" [53], [54].

Another benefit of rsfMRI, in comparison to tfMRI, is its non-engagement in any cognitive task, which can extensively apply to different patient populations [55], [56]. Additionally, several studies suggest the reliability of rsfMRI regarding test-retest reproducibility and inter-subject variability [42], [57]-[59].

FC analysis in rsfMRI has been a popular tool in studying the neural functional architecture of humans [40]. However, several studies have also demonstrated the temporal variability of rsfMRI data [60]-[63], and that FC between brain regions behaves in a meaningful pattern over time [21], [26]. This opens up a popular sub-field of FC analysis named dynamic functional connectivity (DFC). Furthermore, another new perspective on DFC is through the co-activation pattern (CAP), which can be viewed as distinct spatial configurations of brain activity in time. The temporal variability in rsfMRI is partly attributed to the dynamic brain organization that is associated with CAP [26].

Variants of accompanying methods exist for analyzing rsfMRI data, including seed-based approaches [64]-[67], independent component analysis [4], [57], graph methods [50], [68], [69], clustering algorithms [54], [70]-[73], neural networks [74], and pattern classifiers [75], [76].

2.3 Avalanche

2.3.1 Introduction of avalanche

Studies have shown that while at rest, the brain remains in a critical state or criticality [8], [77], [78]. The criticality is a balanced state as the system being neither hyper- nor hypo-excited [79]. Thus, small perturbation from the localized neural activity is likely to cause cascades in neural activity throughout

the brain [8], [12]. Researches show that cascades are organized in spatiotemporal correlated patterns, termed "neuronal avalanches," and information can be formed as trains of avalanches [8]-[10]. By definition, an avalanche is assembling this information or "active" elements (i.e., voxels), regardless of the size or length, over time, surrounded by inactivation [8], [80]. In general, the avalanche and criticality have been of high interest in research fields, especially with the advance in sampling techniques. Tagliazucchi, 2012 [21] proposes an approach to detect avalanches with rsfMRI, which is a hallmark of avalanche investigation.

2.3.2 Avalanche detection with fMRI

(1) Seed-based BOLD signal

Avalanches (or cascades) are in a spatiotemporal form, and traditionally for avalanche analysis in fMRI, the temporal dimension is equally spaced by TR. TR is the time interval between fMRI scans. Tagliazucchi [21] detects avalanches with rsfMRI via a novel point process technique, which extracts a sequence of time points, exceeding a predetermined threshold, from the BOLD signal at a seed region. Then, clusters of contiguous activated voxels were extracted during these thresholded time frames. Avalanches were defined by organizing the clusters that have spatial intersections at subsequent times. Otherwise, the temporal propagation stopped. In this work, Tagliazucchi [21] presents the resting-state activation maps generated from a subset of points in the entire time course, and the results suggest that the brain coactivates at avalanches. Some related studies by Liu [23], [24] also show similar results from applying the seed-based point process technique.

(2) Global level of activity

The work by Tagliazucchi also concludes that the brain remains in a critical state, and as expected for a large-scale critical system, the system undergoes an order-disorder transition at criticality [21]. Thus, Tagliazucchi [21] implies another large-scale avalanche detection approach via tracing the global level of activity, the size of the *largest* cluster, over time. This method applies the point process technique

to the global fMRI signal measure and computes straightforwardly in contrast to other metrics, such as the branching ratio [8]. Additionally, it is also investigated in [27], [28] that the covariation of brain activity may be condensed into a subset of time points in the global fMRI signal at rest.

In our work, we performed the instantaneous whole-brain correlation (IWBC) analysis proposed by [29], which calculates the sum of correlations of voxels throughout the brain at each point in time. Full details, including the calculation, will be discussed in chapter 3. Figure 2.2 shows the normalized global fMRI signals from two metrics (unit norm). As shown, the IWBC coincides with a vast majority of the timing in the global activation measure, denoted as *Max Size* cluster, proposed by Tagliazucchi [21]. The measure of the whole-brain correlation levels behaves similarly to the global activation measure. The few gigantic peaks, "extreme events" in IWBC, also correspond to large co-activation that extends as far as the entire cortex. Thus, applying the global fMRI signal measure, IWBC helps to encode the avalanches in time for analysis in this work.

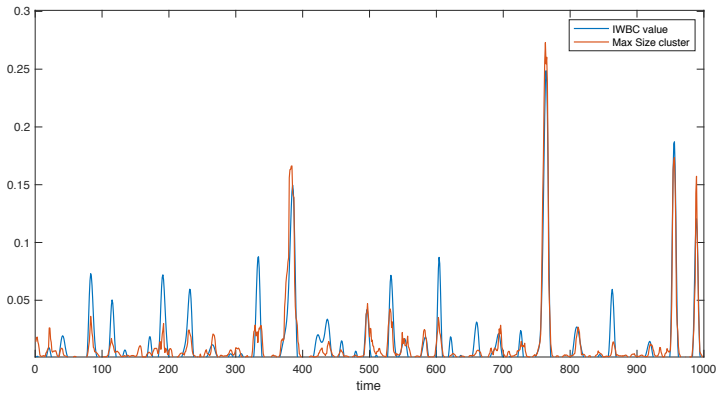

Figure 2.2 Global fMRI signal measure

2.3.3 Avalanche investigation and criticality

Tagliazucchi's work [21] suggests the possibility of compressing an enormous dataset using temporal marks of the BOLD signal via a point process. This approach provides useful clues on

investigating the dynamic organization of brain activity. Some recent works with fMRI signal processing have applied this novel perspective to study the brain behaviors.

In the primary referring resource of the present study, Bell [29] investigates the DFC co-activation patterns (CAPs) and the network connectivity during avalanching vs. non-avalanching periods derived from IWBC calculation. This work concludes that the CAPs at avalanches display more connections between brain regions and also RSNs, and accordingly, suggests the brain activity dominated by avalanches of activity [29].

Apart from the studies in CAP decomposition, recent work by Khairi [81] applies the modified Principle Component Analysis (PCA) and sliding window analysis to investigate the fMRI signal decomposition. This work provides insight into looking at the change of the signal content with continuity from a group of fMRI scans to another. This approach shows that there may be some brain synchronization at IWBC avalanches, where disparate brain regions are highly correlated.

Another vital direction that researchers have been pursued is the investigation of criticality. Avalanches are identified to be near the criticality, and the size of avalanches can be fitted to a scale-free power-law distribution, which is a hallmark of the critical dynamics [82]-[84]. The work by Wiegert [85] further investigates the criticality dynamics and the criteria of power-law fitting in fMRI data. It is a good understanding of the universal law of the brain, instead of investigating *ad hoc* laws and attributing to the specialty of biology [77].

The following of this section introduces an example of criticality dynamics proposed by Tagliazucchi [21]. Figure 2.3 shows the calculation for a single HCP subject. As shown, dots correspond to the fMRI volume calculation at each point in time. On the top of Figure 2.3, it depicts the instantaneous relation between the number of active clusters and the active sites (or equivalently, the number of active voxels) throughout the brain. On the bottom, the order parameter (order P.), which is the normalized *Max Size* cluster*,* is calculated over time

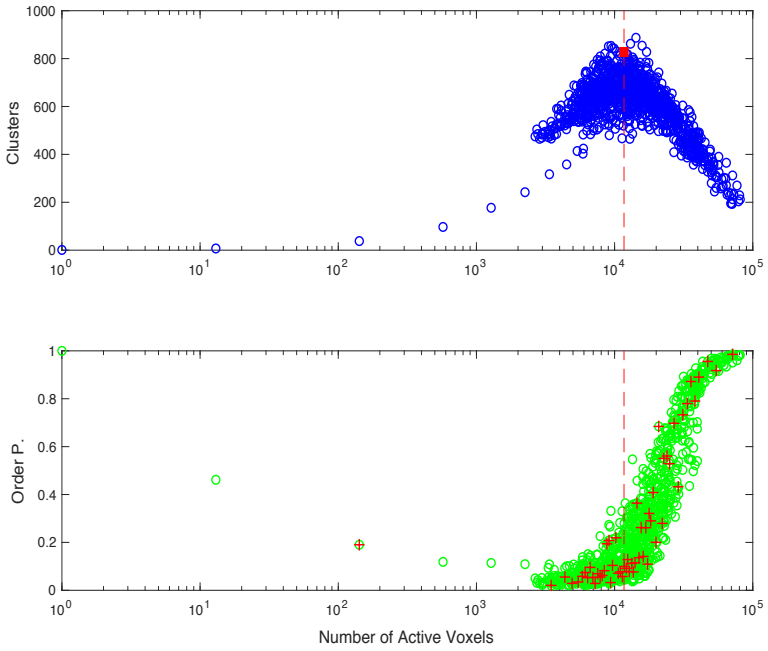

Figure 2.3 Criticality dynamics and Phase transition

As shown on the top of Figure 2.3, the number of clusters reaches a maximum (~800) as well as the variability. The red square and dashed line roughly indicate the criticality value (~12000 total active voxels). It can be seen that above this global level of activity, it shows a reversed correlation between the number of clusters and active voxels. The few gigantic avalanche peaks of high global activation levels are on the right-most tail with a smaller number of clusters, which implies the presence of vast clusters of activation on the cortex.

On the bottom of Figure 2.3, the green dots represent the instantaneous order parameter (order P.) calculation. This parameter expresses the organization of the brain activation, and at each point in time, is defined as the size of the *largest* cluster normalized by the total number of active sites (voxels). For convenience, the crosses in red show the averages given the number of active voxels.

As shown, there is a sharp increase in the order parameter above the critical level (see the red cross), which may imply the presence of an order-disorder transition in brain dynamics. Also, the brain spends most time at or near the critical state. The few avalanching periods of high co-activation are likely to

have high order parameter values close to 1, which infers the growing size of clusters that incorporate most active sites on the cortex.

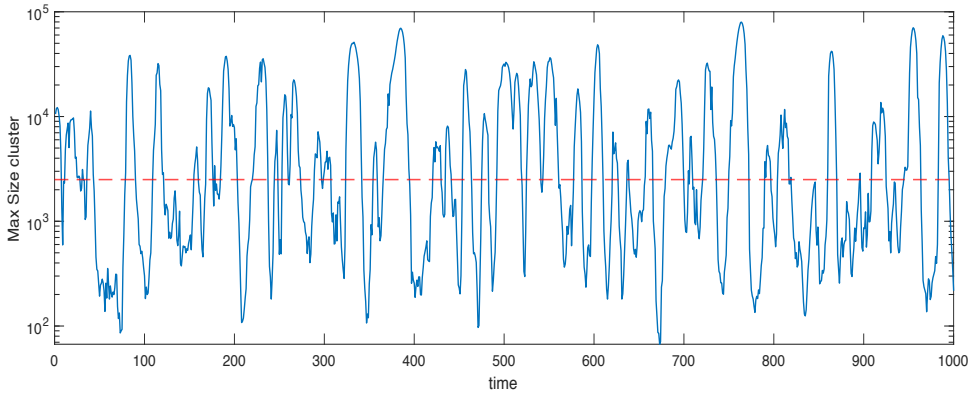

Figure 2.4 Temporal evolution of the *Max Size* cluster

Lastly, Figure 2.4 displays the temporal evolution of the size of the *largest* cluster, denoted as *Max Size* cluster. For this HCP subject, the *Max Size* cluster at criticality is approximately 2500 active sites and shown as the cutoff in red. The brain tends to stay in a critical state as neither hyper- nor hypo-excited. The few cascades of high activation, known as avalanching periods, are induced as brief peaks near the criticality.

CHAPTER 3

METHODS

Chapter 3 mainly describes the methods in processing and analyzing fMRI data in the present study. 3.1 and 3.2 introduce the preprocessing steps to the fMRI data. Then the following 3.3 explains the procedure of CAP methods in detail. Finally, 3.4 provides some data analysis approaches to the output data.

3.1 fMRI data acquisition and preprocessing

Data were provided [in part] by the Human Connectome Project, WU-Minn Consortium (Principal Investigators: David Van Essen and Kamil Ugurbil; 1U54MH091657) funded by the 16 NIH Institutes and Centers that support the NIH Blueprint for Neuroscience Research; and by the McDonnell Center for Systems Neuroscience at Washington University.

The HCP subjects were drawn from a population of 1200 healthy adults (age ranges from 22 to 35 years old). A set of 16 resting-state fMRI data was randomly selected from the HCP database. The HCP image data are of the relatively high temporal and spatial resolution of which subjects were scanned using a customized Siemens Skyra 3T MRI scanner. A gradient-echo EPI sequence for fMRI scanning uses the following parameters: repetition time (TR) = 720 ms, echo time (TE) = 33 ms, image matrix = $104 \times 91 \times 91$ voxels, 72 slices, 1200 volumes (time points), and isotropic voxel size = $2 \times 2 \times 2\ \mathrm{mm}^3$. A full description of the acquisition of data can be referred to [86].

The acquired whole-brain T2*-weighted fMRI data were first preprocessed in the HCP database. Since the fMRI data were scanned given a high spatial resolution and on a scale of millimeters, the subject's body motions could easily affect the fMRI scanning results. These relevant spatial artifacts and

distortions, like head motions, were first removed in the HCP database. Additionally, the HCP database realigned the image data (surfaces and volumes) to standard volume and surface space called MNI space [87]-[89]. Then further pre-processing steps were to remove the low and high frequency noise (e.g., vascular activity or scanner drifts) [85], [89]. The fMRI data were then smoothed by using a finite impulse response (FIR) bandpass filter (0.01-0.1 Hz) and linearly detrended in MATLAB. The reason for choosing this frequency range is to reduce the main effect of physiological noise from heart rates (usually occur at 1.0 to 1.5 Hz) and respiration rates (0.2 to 0.3 Hz) [33]. Due to the computational limitations of the bandpass filtering used in temporal smoothing [29], [81], the first 200 time points (volumes) were then removed from the beginning of the data. The data we used resulted in 1000 time points in length instead of the original 1200 time points from the fMRI scans.

3.2 Instantaneous Whole Brain Correlation (IWBC) avalanche

As previously described in 2.3, "avalanches" can be viewed as temporal marks of the global fMRI signal of which the amplitude corresponds to the whole brain co-activation level. This metric can contribute to analyzing spatial CAPs at each temporal point.

Among different methods of defining avalanches, we performed an instantaneous whole-brain correlation (IWBC) analysis to detect avalanches, which calculated the sum of pair-wise Pearson correlation value of all voxels throughout the brain. Equation 3.1 [29], [81] represents the calculation of IWBC at a single time point n, IWBC[n]:

$$\mathrm{IWBC[n]} = \frac{1}{2}\sum_{i=1}^{N}\sum_{j=1}^{N}\frac{(x_i[n]-\overline{x}_i)(x_j[n]-\overline{x}_j)}{\sigma_i\sigma_j} \tag{3.1}$$

where x_i and x_j are two different voxels, and both i and j iterate over N voxels for $i \neq j$. $\overline{x}$ and σ is the average and standard deviation over the entire time series calculated for a particular voxel.

However, in the present study, we conducted avalanche analysis for positive IWBC signals. It is also noted that the results of using positive signals are similar to using both positive and negative signal values [85]. Thus, we generated a modified IWBC calculation, also denoted as *timescore*. Equation 3.2 represents the modified calculation of IWBC at a single time point n:

$$\text{global mean signal: } gm[n] = \frac{1}{N}\left(\sum_{i=1}^{N} x_i[n]\right)$$

$$\text{IWBC[n]} \approx \textit{timescore}\,[\text{n}] = \begin{cases} gm[n]^2, \text{ if } gm[n] \geq 0, \\ 0, \qquad \text{otherwise.} \end{cases} \tag{3.2}$$

An IWBC time series measures the global correlation level at each time point. Additionally, Figure 2.2 in chapter 2 has shown that the global correlation measure behaves similarly to the global co-activation measure proposed by Tagliazucchi [21]. Therefore, an IWBC series can be applied as a temporal marker for avalanche analysis. Figure 3.1 shows an example of the IWBC plot for a single HCP subject.

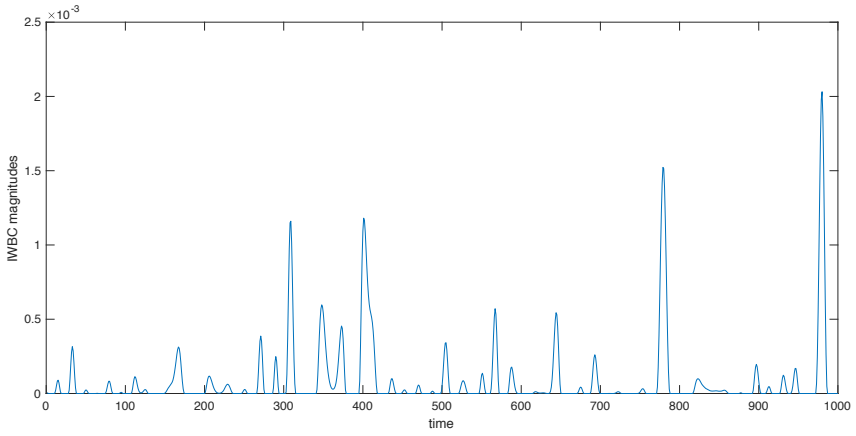

Figure 3.1 An IWBC plot for a single subject

3.3 Spatial clustering of the IWBC series

This section describes the procedure of applying our CAP methods and is organized as follows: 3.3.1 and 3.3.2 are related to some further data processing steps preceding the CAP methods. The following 3.3.3 serves as the primary explanation of the CAP methods used in this work. To conclude this section, 3.3.4 closes with a summary of all steps in the procedure.

3.3.1 Processing BOLD fMRI data to Z-scores volume series

Before investigating spatial CAPs, the preprocessed fMRI data were standardized to the Z-scores volume series with zero mean and unit standard deviation (SD) for each voxel. Thus, the signal value of a voxel at a particular time point directly represents how variant the signal intensity is from the mean (zero) by a certain amount of SD (one).

3.3.2 Spatial CAPs characterization

Once the BOLD fMRI data was processed to the Z-scores volume series, by thresholding and further calculating the volume activity, we extracted the spatial configuration of brain activity, which is the spatial CAPs, at each instant of time. In this work, this process is called spatial CAPs characterization. This characterization then formed a 2D spatiotemporal matrix, which prepared the data before applying our CAP methods. The rest of 3.3.2 provides a detailed explanation of the spatial CAPs characterization.

Thresholding

Figure 3.2 shows the Z-scores thresholding for a voxel series. We set the threshold to be 1.5 SD greater than the mean value (zero) and show as the cutoff in red. Thus, suprathreshold crossings correspond to periods when the voxel is activated; otherwise, it is inactive.

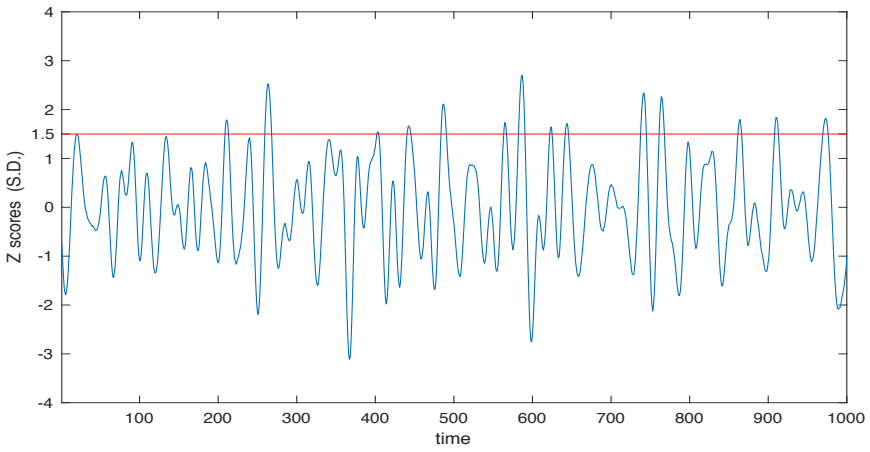

Figure 3.2 Z-scores series of PCC seed for a single subject

Extracting instantaneous spatial features

Following the thresholding, the next step was to obtain the spatial activation at each point in time. In this study, we extracted the instantaneous spatial features (ISFs). Each of the ISFs measures the brain spatial CAPs at an instant of time.

To define the ISFs, Tagliazucchi et al. [21] first utilized clusters of contiguous active voxels for spatial calculation, and the algorithm detecting all connected active voxels can be implemented in MATLAB based on connected component analysis. Given an example, Figure 3.3 presented in [21, Fig. 3A] depicts the temporal evolution of activated clusters (ISFs) in the 2D slice.

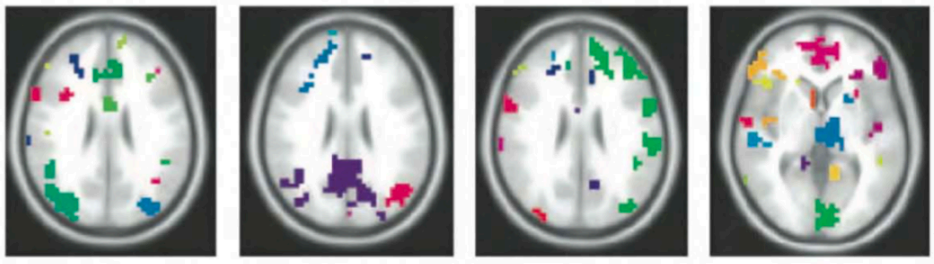

Figure 3.3 Temporal evolution of activated clusters [21]

In this work, however, instead of calculating clusters of connected active voxels, we used *activation size* (the number of active voxels) of particular brain ROIs to define ISFs. The brain ROIs were selected on different brain scales and depending on variants of brain parcellations**.** One advantage of calculating total activity at brain ROIs is that it avoids detecting very tiny clusters and contributes to reducing the dimension of ISFs. Besides, compared to [21], the HCP subjects have a higher spatial resolution, which results in a larger-scale dataset. Thus, the reduction in the spatial dimension of ISFs can also decrease computation time while using a complete dataset. The following section gives an elaborate description of the chosen brain ROIs:

1. Rudimentary brain lobes and cingulate cortex. The first type of ISFs includes the activation size of four major brain lobes (i.e., frontal lobe, parietal lobe, left and right temporal lobes, occipital lobe) and cingulate cortex. These brain lobes were defined purely based on brain anatomical classification but have also been shown to be related to different functions [90]. The total activity of the cingulate cortex was also added into ISFs calculation due to its location. The cingulate cortex is in the medial surface of the brain, where it overlaps with parts of the frontal, parietal, and temporal lobes. Hence, we calculated the activation sizes based on this rudimentary cortical brain map.

2. Brodmann areas (BAs). Brodmann areas defined and numbered by German anatomist Korbinian Brodmann [91] provide a finer level of cortical brain mapping. It has been one of the most frequently cited cytoarchitectural organizations of the human cortex. Also, Brodmann areas, defined based solely on the cytoarchitectural organization of neurons, have been closely correlated to diverse brain functions [92]. Therefore, Brodmann areas combine both anatomically and functionally cortical organization. In this work, we further explore the spatial CAPs within each of the major lobes and cingulate cortex via Brodmann areas.

3. Resting-state networks (RSNs). According to chapter 2, RSNs signify the intrinsic brain organization and functional connectivity under the resting condition. Due to this nature of RSNs, an

RSNs atlas can be seemed as providing contiguous, comprehensive results of brain mapping [93], [94]. Additionally, using RSNs can incorporate the functional perspective of brain activity. In the present study, we used the five major RSNs (default mode [DMN], salience [DMN], central executive [CEN], sensorimotor [SMN], and visual networks [VIS]) derived from the CAREN atlas, a reproducible brain RSNs atlas proposed by Doucet et al. in [95], to approach ISFs.

Spatiotemporal CAPs in 2D matrix form

Following the ISFs extraction at each point in time, a formalized 2D matrix containing spatiotemporal information about brain activity was generalized for our CAP methods. For instance, A vector of ISFs (underlying a rudimentary brain map) at a single time point t is defined as:

$$\mathbf{I}_t = \begin{bmatrix} f_{frontal} & f_{parietal} & f_{temporal} & f_{occipital} & f_{cc} \end{bmatrix}^T$$

This allows a 2D spatiotemporal matrix to be defined as:

$$\mathbf{F} = \begin{bmatrix} \mathbf{I}_1 & \mathbf{I}_2 & \mathbf{I}_3 & \cdots & \cdots & \mathbf{I}_N \end{bmatrix}$$

The spatiotemporal matrix **F** has size M by N, where M is the number of spatial features, and N is the length of fMRI data. Each column vector of F expresses the ISFs calculation at a particular time point, while each row vector represents the temporal evolution of a particular spatial feature.

Regarding the procedures described in this section, preprocessed fMRI data followed the neuronal activation thresholding (Z-scores thresholding), instantaneous spatial features extraction, and spatiotemporal matrix characterization. Thus, the data were collected and prepared to perform our CAP methods.

3.3.3 CAP methods applied to IWBC series

In this work, we used the classical CAP methods described by Liu et al. [26]. We applied a simple k-means method [96] to do spatial clustering temporally on the data (2D spatiotemporal matrix). Column vectors (ISFs) of the spatiotemporal matrix were assigned memberships to 1 of the k clusters (groups)

based on their distance from cluster centers, which in turn are the average of their members. Iterating and updating memberships and cluster centers until required convergence [42], [73]. Consequently, each of the k cluster centers showed the average spatial CAP of all temporal points in that cluster. Also, each time point in the IWBC series then corresponded to an average spatial CAP (cluster center).

Therefore, a connection between observing the global fMRI signal and spatial CAPs can be built via IWBC. More precisely, each time point in the IWBC series can be mapped to its corresponding average spatial CAP. Through this connection, we can further explore the temporal dynamics of the spatial CAPs in the IWBC series. The next section 3.4 will detail the analysis of output data.

In the present work, we employed spatial clustering in the following two cases:

1. Clustering over the entire IWBC series. In this case, all fMRI data contributed to the clustering results. Hence, the spatial clustering grouped all ISFs in the 2D spatiotemporal matrix that correspond to all fMRI volume.

2. Clustering transient points in the IWBC series. Instead of clustering over the entire time series, clustering of ISFs of transient points was performed in this case. The essential idea behind this method was inspired by the point process technique. As described in [21]-[24], brain activity can be studied from brief intervals of high brain coherence. In this case, brief peaks or intervals of high correlation values then constituted the data for clustering. Thus, the data size was substantially reduced to only combine the few sparsely distributed ISFs. Figure 3.4 shows an IWBC plot, where the red asterisks mark all avalanche peaks.

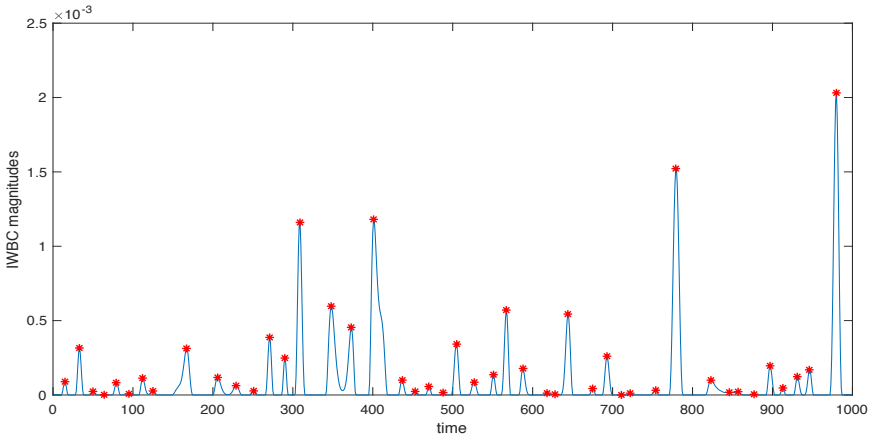

Figure 3.4 The IWBC series with peaks marked

In this work, the points of interest were not detected through a thresholding scheme as proposed by Tagliazucchi [21]. Instead, we merely chose the brief intervals at the few gigantic avalanche peaks for clustering. Thus, only the few "extreme events" in the IWBC series comprised the dataset. Additionally, the length of the interval must satisfy the detection of high local activation. Considering there might be hemodynamic delays in cortical brain regions (which may last up to 2 to 4 seconds) to these peaks, we set both ends of the intervals to be 4 seconds (roughly 5 TRs, TR = 720 ms) from the centers, which are avalanche peaks. TR is the sampling interval for fMRI scans.

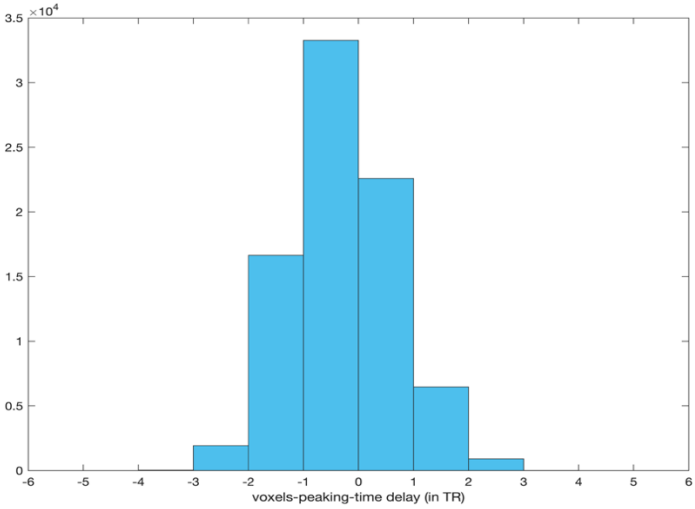

Figure 3.5 Histogram of voxels-peaking-time delays

As a validation, the timing of voxels reaching local peak activation was calculated throughout the brain. The histogram (see in Figure 3.5) shows the averages of voxels-peaking-time delays to the 20 tallest peaks in IWBC. It reveals that over 99% of voxels' peak activation can be captured within the interval. We repeated the same validation process across other subjects and approached consistent results.

3.3.4 Summary of Procedure

To summarize the CAP methods, the procedure begins with the initial brain activity identification via Z-scores thresholding. At each point in time, the thresholding captures the voxel-wise brain spatial CAPs. To reduce the computational time and complexity, the following step, spatial CAPs characterization, is then performed. In this step, spatial features that characterize the brain spatial CAPs are defined and computed as the input data for subsequent CAP methods. Lastly, the k-means clustering algorithm is then applied to classify the spatial CAPs into k clusters. In terms of the clustering, two perspectives are provided, which are clustering over the entire series and clustering of transient points of highly organized brain activity.

3.4 Data interpretations

To better interpret the output data from the spatial clustering, this section provides the data analysis methods in this work: (1) 3.4.1 involves the analysis of CAP decomposition, also defined as state decomposition. (2) The following 3.4.2 provides further analysis, where a probabilistic Markov Model (MM) is formed to interpret the temporal dynamics of spatial CAPs (brain states) in the IWBC series.

3.4.1 State decomposition of whole-brain activity

After applying the k-means method temporally on the fMRI data processed in 3.3, the whole-brain activity can be decomposed to k distinct brain states corresponding to k clusters of spatial CAPs. Then we used the cluster centers, which represent the average patterns of their clusters, for analysis. For convenience, we labeled the brain states or spatial CAPs by positive integers. Positive integers (1 to k)

with state k quantifying the most active spatial CAP and state one being the quietest. This quantification was done by computing a simple L2 norm of each distinct spatial CAP.

Figure 3.6 shows an example of the output data, where Spatial Feat expresses the spatial features such as the activation size of a particular brain lobe or Brodmann area. As shown, a dynamic sequence of states can map each temporal point in the IWBC series to a spatial CAP.

IWBC value (global fMRI signal)

↕

IWBC time index: [t_1 t_2 t_3 ⋯ ⋯]

↕

State sequence: [i j k ⋯ ⋯], k is the maximum

↕

	Spatial Feat 1	Spatial Feat 2	Spatial Feat 3	……
State 1	----------Spatial CAP 1----------			
State 2	----------Spatial CAP 2----------			
⋮				
State k	----------Spatial CAP k----------			

Figure 3.6 IWBC brain states mapping to spatial CAPs

Further analysis of the output data includes:

1. Synchronization of brain co-activation. By mapping IWBC values to spatial CAPs, we can investigate the correlation between global fMRI signal and spatial activation. Additionally, through the spatial CAPs observation, we can also study the synchronization of brain co-activation across spatial brain regions (e.g., major brain lobes, Brodmann areas, and RSNs). Through the temporal marker we can visualize the spatial CAPs and their changes at IWBC avalanches.

2. Point process investigation. In the present study, the spatial clustering was done in two ways as we previously described. Then the generating two groups of spatial CAPs account for two types of clustering. By measuring the similarity between these two groups, we can evaluate the effect of the point process technique. Following Tagliazucchi et al. in [21], in the present investigation, we chose RSNs maps for evaluation.

3.4.2 Interpretation of the temporal dynamics via Markov Model

Following the state decomposition, we derived a sequence of positive integers, each of which links to distinct k brain states (spatial CAPs). Then, a stochastic Markov Model (MM) was introduced to explore the temporal dynamics of brain states by interpreting this sequence of integers. Each of the integers itself symbolizes a state in MM and thus is assumed to follow the Markov chain process with a finite state space (size = k). Moreover, to understand the temporal dynamics, MM automatically generates a transition matrix that formulates a probabilistic interpretation of the temporal transition among states. A detailed description of MM and its applications can be referred to [30].

Markov property

According to [30], the defining characteristic of MM can be summarized that the state has a one-step memory. In other words, the present state is only dependent upon the state observation at the previous time step. This precisely defined characteristic is also called Markov property. Generalizing from [30], let the sequence $X_1, X_2, \dots, X_N$ of random variables, known as a discrete Markov chain, demonstrate this stochastic process. The values of random variables are possible recorded states. Markov property can be expressed by a sequence of random variables satisfying conditional independence. An example is provided in Equation 3.3:

For any positive integer n and possible states $i_1, i_2, \dots, i_N$ of random variables,

$$P(X_n = i_n \mid X_{n-1} = i_{n-1}) = P(X_n = i_n \mid X_1 = i_1, X_2 = i_2, \dots, X_{n-1} = i_{n-1}) \qquad (3.3)$$

Since the k-means clustering algorithm is unsupervised learning of brain CAPs, clustering is based on the instantaneous spatial activation characteristic regardless of temporal locations in the global fMRI signal. Similarly, to study its temporal dynamics, the knowledge of the previous state is all that is necessary to determine the present state, which satisfies the Markov property.

Thus, by using the derived sequence of state integers as the input to MM and counting state transitions for every consecutive pair over the entire state sequence, we can approach the temporal transition probabilities among states via the transition matrix.

Transition matrix

The temporal transition probability between states can be denoted as conditional probability $P(X_{next} \mid X_{present})$. $X_{present}$ and X_{next} denote the random variables for the present and next states, respectively. For a k-state Markov chain, both values of random variables $X_{present}$ and X_{next} can span the state space, which are integers ranging from 1 to k. Thus, $P(X_{next} \mid X_{present})$ can be expanded to a k-by-k matrix form containing all information on these probabilities. This matrix, denoted as $\mathbf{P_{tr}}$, is then defined as:

$$\mathbf{P_{tr}} = \begin{pmatrix} P(X_{next}=1 \mid X_{present}=1) & P(X_{next}=2 \mid X_{present}=1) & \cdots & \cdots & P(X_{next}=k \mid X_{present}=1) \\ P(X_{next}=1 \mid X_{present}=2) & P(X_{next}=2 \mid X_{present}=2) & \cdots & \cdots & P(X_{next}=k \mid X_{present}=2) \\ \vdots & \vdots & \ddots & & \vdots \\ \vdots & \vdots & & \ddots & \vdots \\ P(X_{next}=1 \mid X_{present}=k) & P(X_{next}=2 \mid X_{present}=k) & \cdots & \cdots & P(X_{next}=k \mid X_{present}=k) \end{pmatrix}$$

Directed graphs

In this work, we used the traditional MM, and thus the transition matrix generated is independent of time. For better visualization of the transition matrix, we also introduced directed graphs for analysis. Vertices of a directed graph are states in the k-state MM, and the probabilities of transition among states label edges. Additionally, a vertex's connectivity (or the number of connections) is thought to measure

the complexity regarding the state switches. Then, several critical nodes (vertices) with higher local connections can be observed and further investigated.

Direct visibility

Unlike the Hidden Markov Model (HMM) and other methods, one advantage of using MM is its direct visibility of states. The states are integers quantifying the activation level of spatial CAPs, and accordingly, the temporal transition of states can be directly visible to observers.

CHAPTER 4

RESULTS

Chapter 4 presents the results of the study as follows: 4.1 and 4.2 are related to brain state decomposition via our CAP methods. The former focuses on applying clustering over the entire fMRI series, while the latter utilizes the point process technique by clustering over only transient intervals in the IWBC series. 4.2 also includes an evaluation based on this novel technique. Then this is followed by 4.3, which provides the results of MM in studying the temporal dynamics of CAPs.

According to the configuration settings of this work, the well-developed k-means method was used for clustering (iteration times: 1000). However, the only free parameter that affects the clustering results is the number of clusters (k). To thoroughly study brain states, we examine this parameter k from 5 to 10. The fMRI data are based on the cortical brain surfaces, which are mainly gray matter cortical regions. Also, as described in chapter 3, the CAREN atlas proposed by Doucet et al. in [63] contains the parcellation of five major RSNs (default mode [DMN], salience [DMN], central executive [CEN], sensorimotor [SMN], and visual networks [VIS]). These networks are included in section 4.2 to show the results of applying the point process technique vs. clustering over the entire fMRI series. In section 4.3, the configuration settings of the MM depend on k, and we extended the choice of k to k = 5, 10, 15 for comparison. Finally, for the sake of consistency, the figure and tables shown in the rest of this chapter are all from the same single fMRI subject. These are then followed by the summarized results accounting for all fMRI data in this work.

4.1 State decomposition over the entire fMRI series

4.1.1 State decomposition based on major brain lobes and cingulate cortex

Figure 4.1 shows the visualization of brain state decomposition based on the four rudimentary brain lobes and the cingulate cortex (the number of states is k = 8). Using IWBC as a temporal marker shown in Figure 4.1 (a), each point in time is marked with a state number, and the state number itself quantifies the activeness of the related spatial CAP. Thus, we can not only observe the global fMRI signal value but also directly see the brain states for time points. As shown, the high IWBC values (at tall peaks) are likely to have high state numbers, and similarly, low IWBC signal values (at small peaks) usually relate to small state numbers. Also, the time points near tall IWBC avalanche peaks have relatively higher state numbers. From Figure 4.1 (b), in a spatial perspective of visualizing the CAPs of brain states, the spatial CAP for each state number is represented by the generated cluster center. What is interesting about the results is that we can observe a general pattern that the activation of spatial CAPs mostly behaves as scaling up and down together across defined anatomical regions. To be more specific, given the frontal lobe as an example, the order of the local activation level in the frontal lobe is in line with the activation level of spatial CAPs (brain states). We ran the experiment on all fMRI subjects in this work and found this pattern to be consistent in spatial CAPs. This alignment then indicates that the activation at these brain regions synchronizes with the activation of brain states. Overall, these results from Figures 4.1 (a) and (b) indicate:

(1) Our correlation-like global fMRI signal measure, IWBC, can generally reflect the activeness of brain states. The big avalanche peaks usually correspond to most active brain states (spatial CAPs).

(2) By taking a rudimentary level of the whole-brain cortical map (e.g., four major brain lobes and cingulate cortex), the map components are likely to activate and deactivate synchronously with the activeness of brain states in the IWBC series.

In summary, underlying this rudimentary brain mapping, the activation synchronization exists throughout the brain.

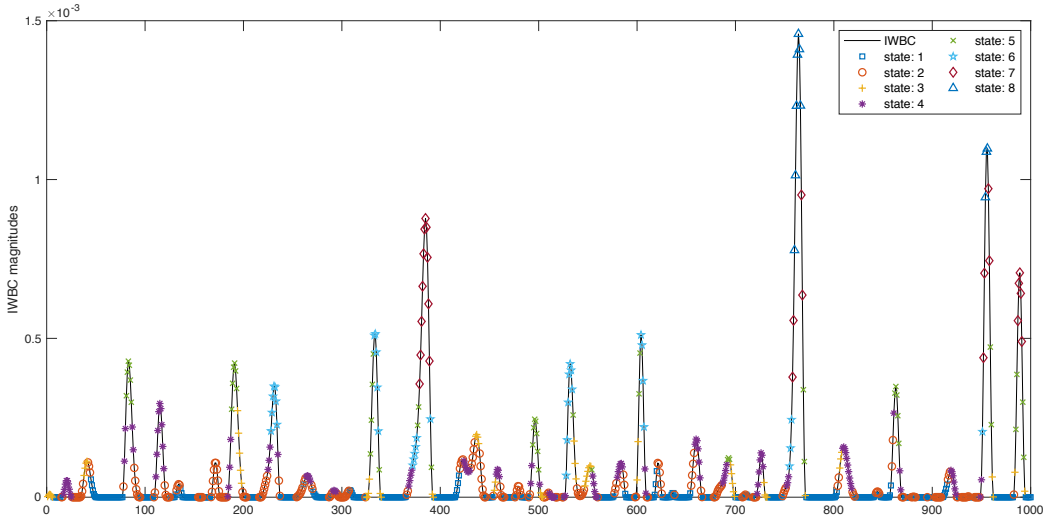

(a) Temporal visualization: Decomposed brain states in the IWBC series

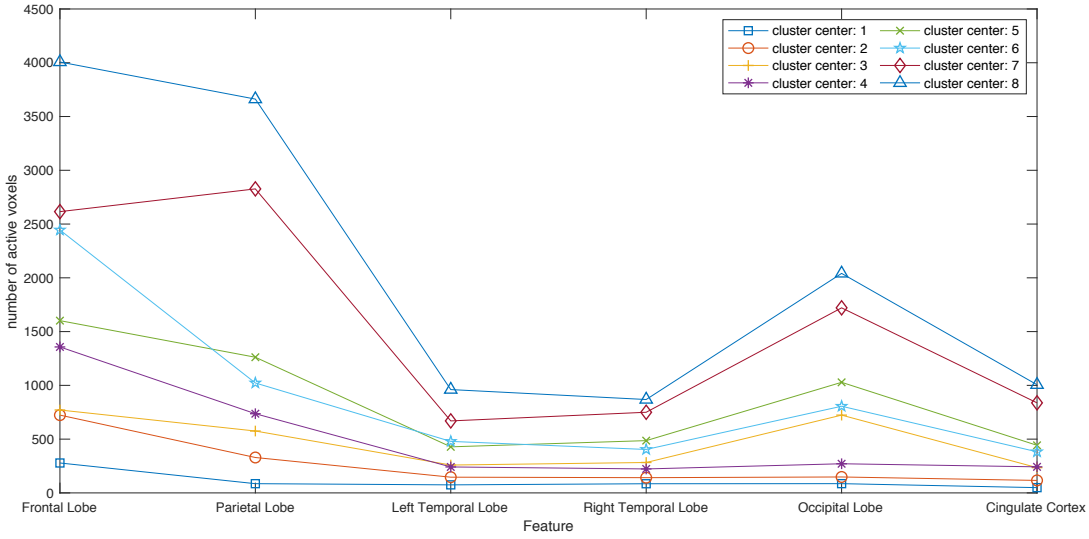

(b) Spatial visualization: Spatial CAPs that linked to distinct brain states

Figure 4.1 State decomposition based on major brain lobes and cingulate cortex

4.1.2 State decomposition based on Brodmann areas

The previous section presents the clustering results underlying a rudimentary whole-brain cortical map. To further analyze the data, this section moves on to discuss the results on a more precise anatomical map, Brodmann area. We performed clustering within each of the brain lobes and the cingulate cortex. Considering the general activation and the spatial location of these brain regions in

fMRI data, we display the clustering results of the parietal lobe (active), occipital lobe (medium active), and also cingulate cortex (middle brain) in Figure 4.2.

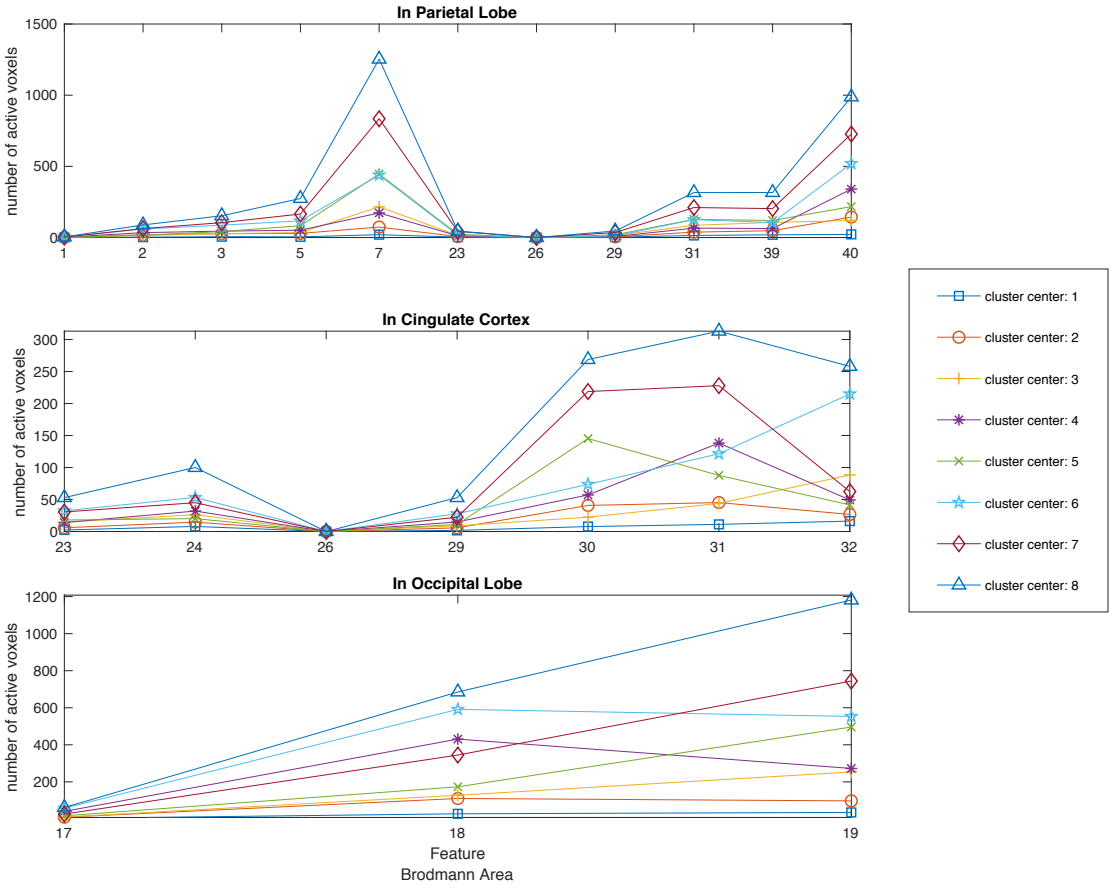

Figure 4.2 State decomposition based on Brodmann areas

Similar to Figure 4.1 (a), within each lobe or cingulate cortex, the IWBC values can generally reflect the activation level of brain states. Thus, in Figure 4.2, we only present the spatial visualization of clustering results, which are spatial CAPs.

As can be seen from Figure 4.2, by applying a more precise anatomical map, we can still observe a similar pattern as described in 4.1.1 in most Brodmann areas. In Figure 4.2, the set of spatial CAPs of the parietal lobe gives a promising demonstration. Most Brodmann areas are likely to activate together as the state number increases. However, there are some pairs of Brodmann areas that act differently.

Given the cingulate cortex as an example, comparing the Brodmann area 31 (posterior cingulate cortex [PCC]) and 32 (anterior cingulate cortex [ACC]) with other areas, it is evident that the spatial CAPs do not follow a similar pattern of scaling up and down together. Instead, spatial CAPs show "crossings" in these two Brodmann areas as the brain state changes. As the whole-brain activation level increases (i.e., in the spatial activation map, state 6 to state 7), the local activation of PCC becomes dominant. At the same time, the ACC falls off from being very active. The same pattern also exists in the occipital lobe as Brodmann area 18 (secondary visual cortex [V2]) and 19 (associative visual cortex [V3, V4, V5]).

By repeating the same procedure throughout the entire set of HCP subjects in this work, we then summarized all pairs of Brodmann areas that display the consistent asynchronous local activation change. The numerical labels of these Brodmann areas are listed below:

1. Frontal lobe: 9 (dorsolateral prefrontal cortex [DLPFC]) and 10 (anterior prefrontal cortex [aPFC]), 6 (premotor cortex and supplementary motor area) and 8 (includes frontal eye fields).

2. Parietal lobe: 39 and 40 (both considered by some to be part of Wernicke's area)

3. Temporal lobe: 21 (middle temporal gyrus) and 22 (part of superior temporal gyrus, included in Wernicke's area), 37 (fusiform gyrus) and 38 (temporopolar area).

4. Occipital lobe: 18 (V2) and 19 (V3, V4, V5).

5. Cingulate cortex: 30 (subdivision of retrosplenial cortex), 31(PCC) and 32 (ACC).

To summarize, these results suggest that under a more refined brain anatomical map, the spatial CAPs still maintain the general pattern of synchronization, as we derived from 4.1.1. However, when brain states are increasingly active (at medium and tall IWBC avalanche peaks), there are some brain regions in the spatial CAPs that sharply dominate the local activation or instead immediately go quiet. These regions are listed above as Brodmann areas, including some parts of the cingulate cortex (PCC and ACC), prefrontal cortex (PFC), visual cortex (V2, V3, V4, V5), and Wernicke's area. Since the relatively higher IWBC values only occupy a significant portion of the temporal duration, these results showing the

difference in spatial CAPs might provide insight into the study of avalanche peaks, which might in turn potentially present more time-varying information about the brain.

4.1.3 State decomposition based on RSNs

As a complement to 4.1, we also performed spatial clustering based on the CAREN atlas. Compared to the anatomical maps in the previous section, the components of this functional atlas are five major RSNs. According to the resulting spatial CAPs shown in Figure 4.3, overall, we cannot identify the general pattern of synchronization across RSNs. Instead, some components (networks) dominate regardless of the activation level of brain states. One understanding of this form of local activation disorder might be because the spatial features we used are functional networks, we can consider the spatial CAPs as distinct brain functional maps. Then these maps express the functional perspective of brain activity, which increases the variability of local activation in spatial CAPs. Additionally, through inspecting these activation maps at medium and tall avalanche peaks, the spatial CAPs likely change after the avalanche peaks. Regarding avalanche propagation, it undergoes a more broadly activated pattern before reaching its peak; after, it deactivates and turns into a very different spatial activation pattern. Finally, it is also interesting to note that the spatial CAPs can, at least partly, express the nature of RSNs. The DMN (task-negative) displays opposing activation patterns in comparison to some attentional networks, such as SMN and VIS (task-positive).

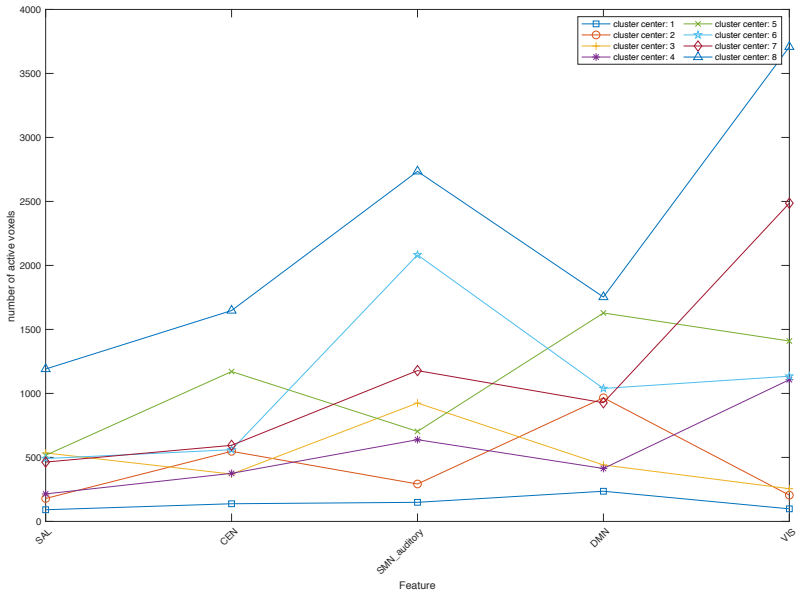

Figure 4.3 State decomposition based on five major RSNs

4.2 State decomposition over transient intervals

The goal of this results section is to investigate the point process technique. As we derived from 4.1.3, apart from a noticeable difference in the general activation level, using RSNs also produces more distinguishable local activation patterns in spatial CAPs. The more unique spatial CAPs then provide convenience for comparing the results from the two types of clustering methods. Thus, the results of section 4.2 are all based upon the CAREN atlas.

4.2.1 Transient intervals extraction

Figure 4.4 shows the extraction of the "outlying events" in the IWBC series. The point process in this work extracts brief intervals at the five tallest avalanche peaks. As shown, asterisks mark the transient intervals. Given the third tallest avalanche peak as an example, the peak is in red in the middle of the time frame, and five temporal points are in blue on each side of the peak. In contrast to the original clustering method, the data then reduce to 55 time points in length (less than 6% of fMRI data).

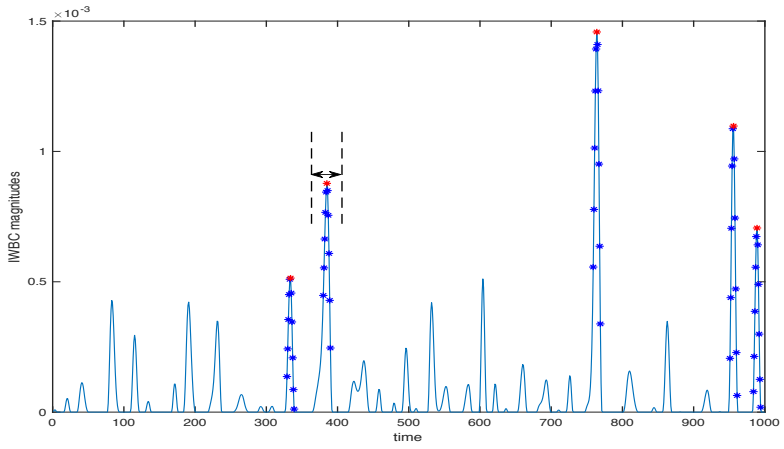

Figure 4.4 Transient intervals extraction

4.2.2 Evaluation of the point process technique

Figure 4.5 shows the results of clustering in our temporal marker (IWBC series) in which the distinct brain states mark time points. As can be seen in both Figures 4.5 (a) and (b), the marked time points can cover the minimum and maximum of the global fMRI signal magnitude. We can also see that the extracted intervals participate in almost all neural events that have IWBC magnitudes over 5.0E-4 (~33% of the maximum IWBC value). This coverage suggests a possibility of studying the time-varying brain activity through only the few brief IWBC intervals.

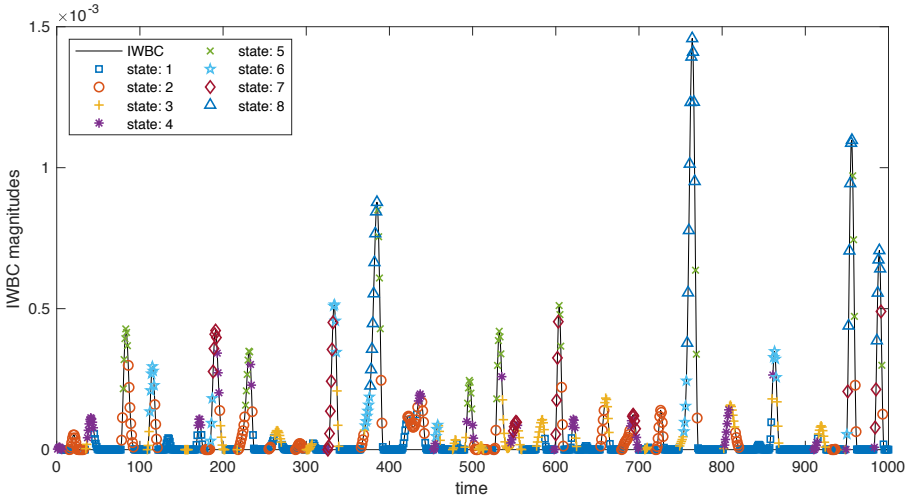

(a) Clustering over entire fMRI series

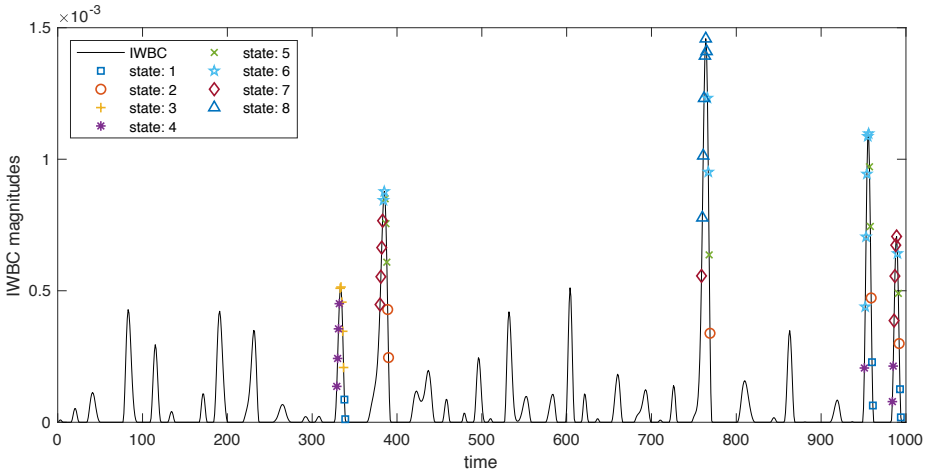

(b) Clustering over transient intervals

Figure 4.5 Temporal visualization of two types of clustering methods

To evaluate the effects of the point process technique, we divide the global fMRI signal into several levels. This division is done by simply looking at the magnitudes of the avalanche peaks. We then observe the spatial CAPs at each global fMRI signal level and see if, under the same signal level, a pattern similar to the one found in the original clustering can be retrieved from clustering these transient intervals.

Table 4.1 is a reference table that summarizes the pairs of spatial CAPs matched at each global fMRI signal level for a single subject. The brain state number is used as the CAP index for simple representation. Meanwhile, the spatial visualization of these pairs is displayed in Figure 4.6. As shown for each pair, the spatial CAP from clustering transient intervals is overall more active than the previous clustering result. This improving general activation is due to the temporal locations of the extracted intervals, which are near the few gigantic avalanche peaks. Accordingly, the results are less likely to overlook high brain activation in fMRI data. We can also see in Figure 4.6 that for each pair, the similarity can be observed as activation synchronization across the five major RSNs. Taking the results from Table 4.1 and Figure 4.6 together, the degree of variability between the results is 13%, which means

that for this single subject, seven spatial maps can be retrieved from only clustering five transient intervals in the IWBC series. By repeating the same procedure for all HCP subjects in this work, we then summarize an average degree of variability (40%) between the two types of clustering methods. Hence, less than 6% of fMRI data preserves 60% of the information on average for representing brain CAPs.

In summary, section 4.2 gives a perspective of applying only a subset of global fMRI signals to study brain spatial CAPs. These results reveal the significance of brain co-activation patterns at the few gigantic avalanche peaks that preserve more time-varying information about brain activity. Also, it suggests that the novel point process technique might be useful in a way comparable with the traditional CAP method.

Table 4.1 The reference of spatial CAPs pairs between two types of clustering methods. Each row of the table expresses a pair of spatial CAPs (shown as CAP index) that are alike in terms of the activation pattern. The global fMRI signal measures the whole brain co-activation and is then listed from active to quiet below. Each pair of spatial CAPs is built up based on their similarity at a particular signal level. The degree of variability is the percentage of unmatched spatial CAPs in the results of clustering over the entire fMRI series.

Global fMRI signal level	**Original CAP index (over the entire series)**	**Referred CAP index (transient intervals)**
1st and 2nd tallest peaks: 1.0E-3 – 1.5E-3	8	8
3rd and 4th tallest peaks: 5.0E-4 – 1.0E-3	5	5
Medium and small peaks: 1.0E-4 – 5.0E-4	7	4
Medium and small peaks: 0 – 5.0E-4	6	3
Medium and small peaks: 0 – 5.0E-4	4	4
Small peaks (quiet): 0 – 3.0E-4	2	2
Small peaks (quiet): 0 – 1.0E-4	1	1
Total	Variability: 1 – 7/8 = 13%	

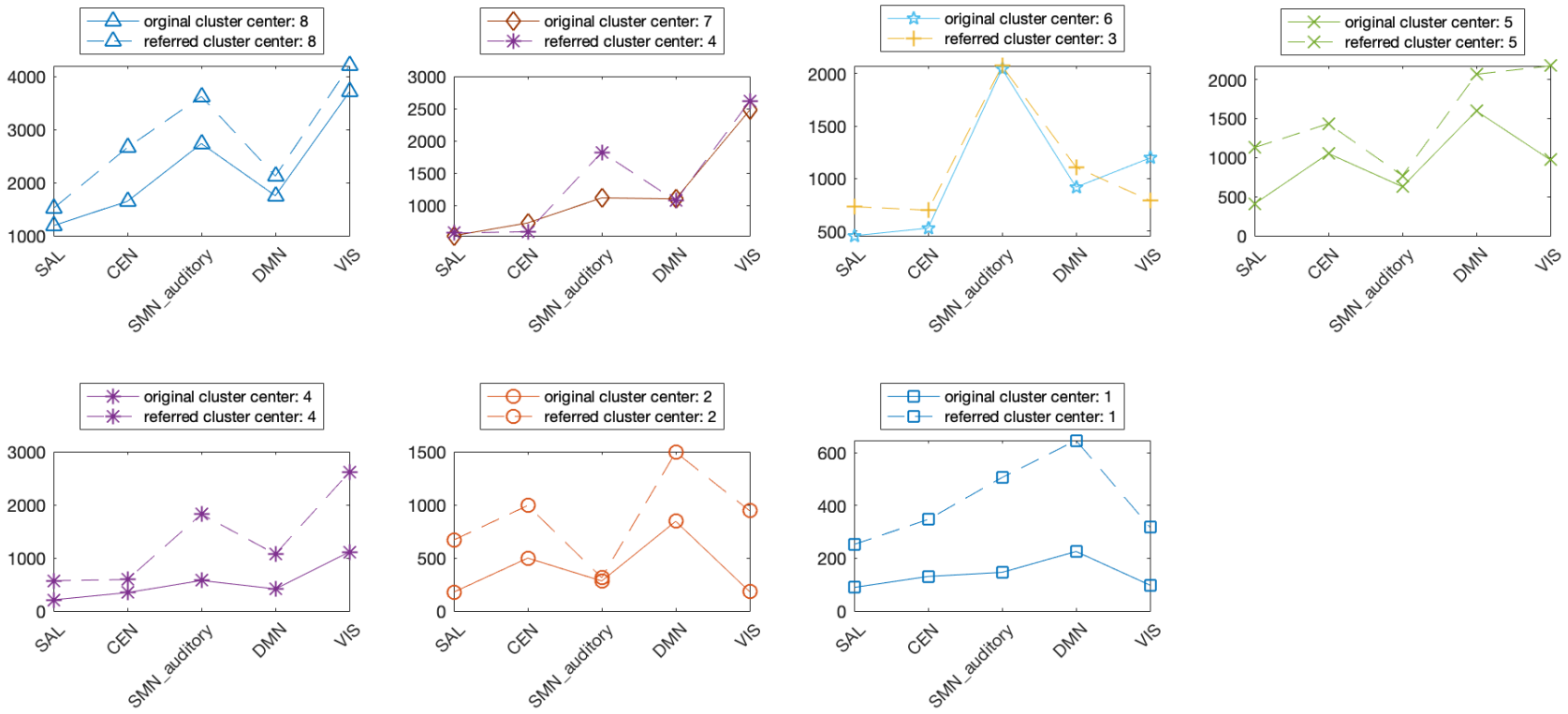

Figure 4.6 Visualization of the spatial CAPs pairs

4.3 MM temporal dynamics identification

As a result of the clustering, a dynamic sequence of brain states or spatial CAPs is generated in the IWBC series. In this chapter, the previous sections 4.1 and 4.2 discussed the results from a spatial perspective, while the present section will further study the temporal dynamics of the brain states. The k-state MM produces output in a transition matrix format, which automatically formulates a probabilistic interpretation of the switches and consistency of brain states. As the configuration settings specify, the choice of k is k = 5, 10, 15. For convenience, we display the results underlying the parietal lobe. Subsequently, the summary accounting for other spatial features in the present study will be provided.

(1) k = 5

Figure 4.7 shows the transition probabilities among states by a directed graph (k = 5). Vertices and edges are states and transition probabilities, respectively. As can be seen, at a time step, the brain states generally have a higher probability of switching to the same state. Especially for the most active state (state 5) and the quietest state (state 1), these probabilities are significantly higher (around 0.9). Besides, we can also see that states 1 and 5 have fewer edges than the medium states (states 2, 3, 4). Both of these initial observations suggest that when k = 5, the brain states, which usually occur at very tiny and big avalanche peaks, have a consistent pattern of switching to the same brain states in the IWBC series.

In Figure 4.8, the transition probability, $P(X_{next} \mid X_{present})$, can be generalized into a binary condition at each present state, which is $X_{next} = X_{present}$ or $X_{next} \neq X_{present}$. As illustrated, at each category (state), the blue column means switching to the same state, and the orange accounts for switching to the rest of the states. Looking at each state in Figure 4.8, states 1 and 5 have a greater difference in terms of these two kinds of transition probabilities. This observation agrees with the finding in Figure 4.7 that when k = 5, each of the states generally tend to switch to the same state, and the very tiny and big avalanche peaks have a significantly high transition probability to the same states.

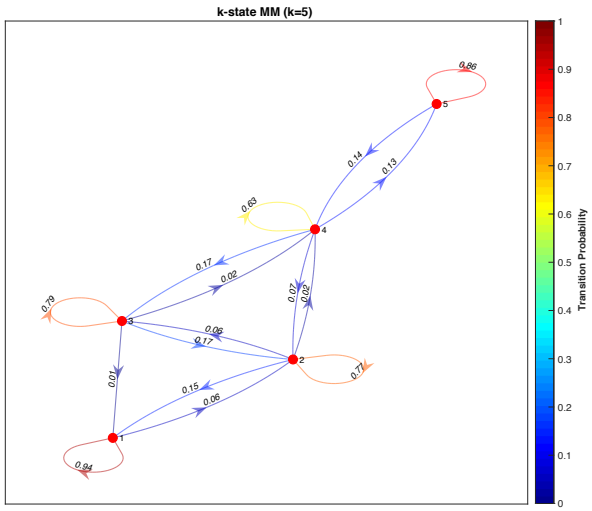

Figure 4.7 Directed graph of the k-state MM (k = 5)

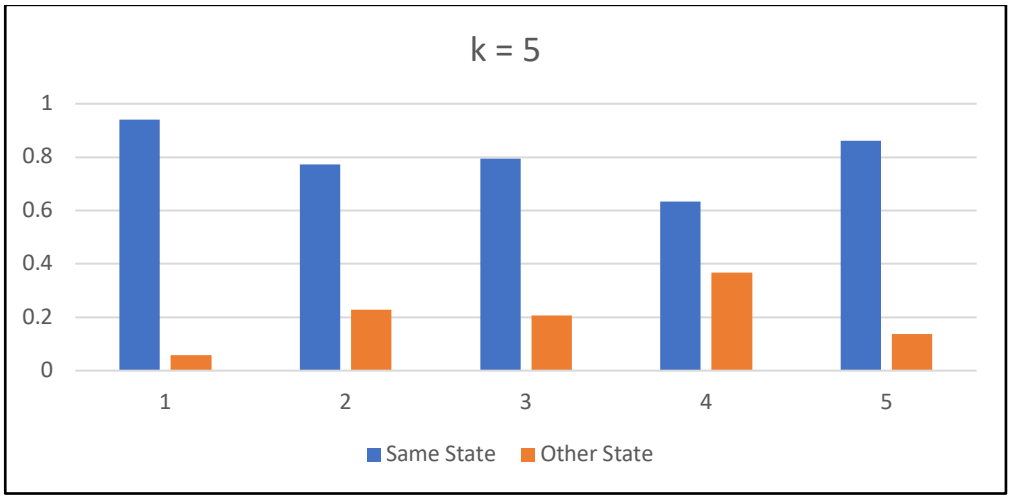

Figure 4.8 Transition probabilities at each state (k = 5)

(2) k = 10

Figure 4.9 presents the output of the k-state MM when k = 10. Similar to what we have observed when k = 5, in both Figures 4.9 (a) and (b), the very active and quiet states have a significantly higher probability of remaining consistent. 0.82 and 0.94 correspond to states 10 and 1, respectively.

Also, to study the temporal switches of the states in MM, we further analyze the directed graph. The routes in (c) and (d) in Figure 4.9 are traversed back from state 10. Since we are observing the switches

between different states, the self-loop does not count for each vertex. In (c), only rising edges are displayed, showing the dynamic switches from inactive to active brain states. The (d) with only falling edges illustrates the dynamics from the opposite direction. Vertices of input degree greater than 2 in (c) and of output degree greater than 2 in (d) are indicated in blue.

As shown, unlike the blue vertices, either the input degrees in (c) or output degrees in (d) for each of the vertices 8, 9, 10 are one. For each of the routes, the vertices on the left (8, 9, 10) are less interconnected than the vertices on the right side. Then, this implies the presence of a subgraph in the state map where the few state vertices on the left side have a more organized switch pattern than the vertices on the right side. Given (c), for instance, when the states rise above 7, the vertices then show lower connectivity (or a lower number of connections), and hence the switches of states become less varied. The vertices on the right, otherwise, are more interconnected and complex in terms of the switch pattern. These results overall suggest that there is a transition among brain states based on their complexity of switch pattern. Some critical nodes, medium active states 6 and 7, for instance, act as hubs in regard to this transition.

By visualizing these critical state nodes in our temporal marker, when k = 10, this transition (e.g., at medium states: 6, 7) tends to occur at temporal points of IWBC values lower than 5.0E-4 (medium peaks). Above this cutoff, the temporal points are likely to have more organized brain states. The most active brain state at the few gigantic avalanche peaks has both organization (less complexity) and consistency.

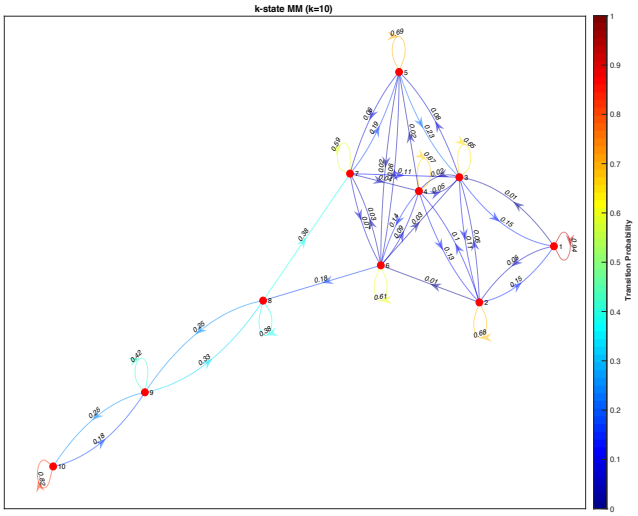

(a) Directed graph of the k-state MM (k = 10)

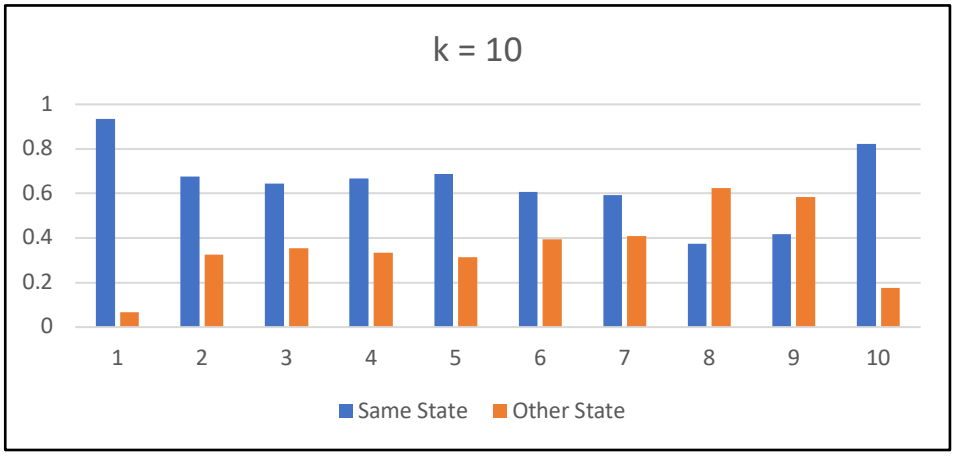

(b) Transition probabilities at each state (k = 10)

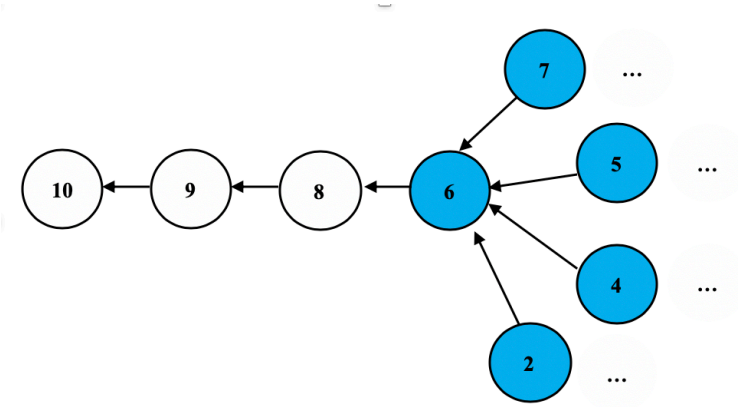

(c) Routes from inactive to active brain states

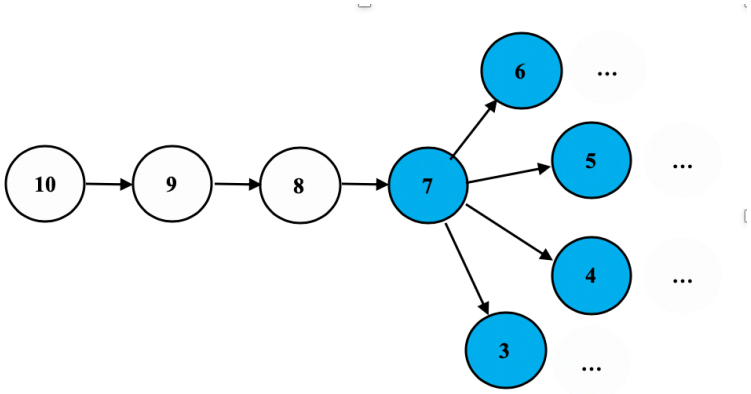

(d) Routes from active to inactive brain states

Figure 4.9 The k-state MM (k = 10)

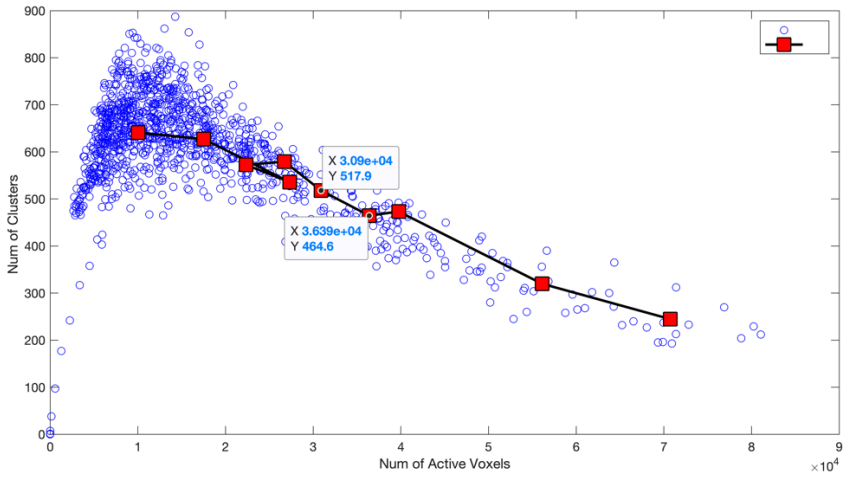

Figure 4.10 Criticality dynamics map

Lastly, Figure 4.10 represents the criticality dynamics, which is also shown in Figure 2.3 in chapter 2. Blue dots represent the calculation at each time point. Red squares, however, represent the averages regarding each of the states and are lined up in order. It is noted that the marked medium states (i.e., critical nodes 6 and 7 in Figure 4.9) are on the right above the criticality (~12000 voxels), and increasing activation leads to organized brain states (i.e., nodes 9 and 10 in Figure 4.9) on the right-most tail of this criticality dynamics map.

(3) k = 15

When k increases to k = 15, we can still see in Figure 4.11 (b) that the tiny and gigantic avalanche peaks (states 1 and 15, respectively) are significantly more consistent than most of the other brain states. Moreover, as illustrated in Figure 4.11 (a), the state vertices on the bottom left are noticeably more organized and less interconnected than those on the top right. When brain states rise above the critical node, state 11, the states generally have less complexity in the switch pattern.

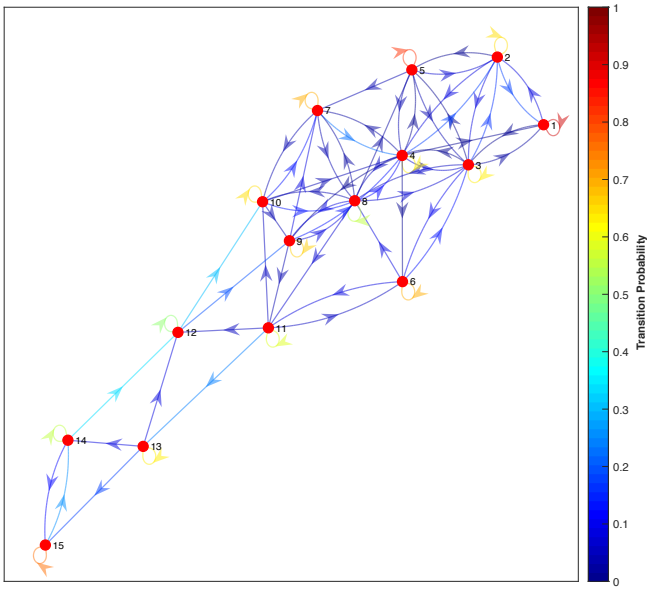

(a) Directed graph of the k-state MM (k = 15)

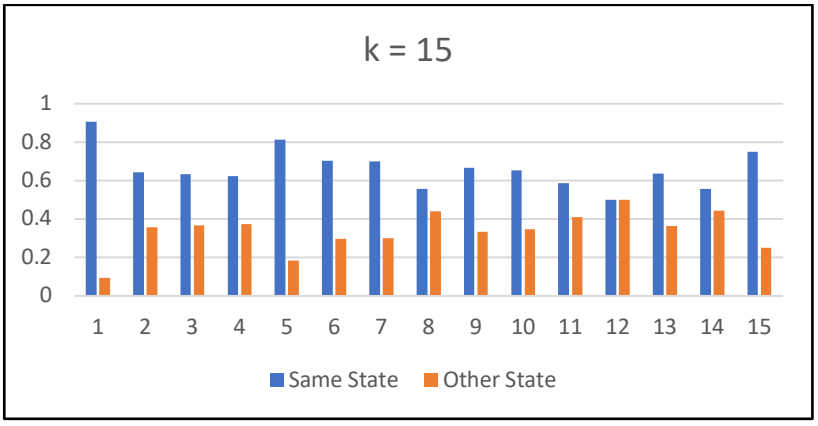

(b) Transition probabilities at each state (k = 15)

Figure 4.11 The k-state MM (k = 15)

Similarly to when k = 5, 10, this transition (e.g., medium states: 6 - 11) tends to occur at temporal points of IWBC values lower than 5.0E-4 (medium peaks) for this single subject. Organized brain states are on the right-most tail of the criticality dynamics map. In conclusion, these temporal dynamics of the brain states in the parietal lobe are consistent in the choice of k.

(4) Summary of the temporal dynamics

Following the observations of temporal dynamics mapped to the parietal lobe, we then repeated the same procedure underlying the whole brain map and RSNs. Subsequently, we ran the experiment on all HCP subjects in this work. In summary, these temporal dynamics are consistent across different subjects and brain maps:

1. States (spatial CAPs) Consistency. In the IWBC series, the brain states at the very tiny and gigantic avalanche peaks remain significantly more consistent. In other words, at a time step, the brain states at these temporal points are likely to switch to the same state.

2. Organized switch pattern. The brain states can be divided into two groups depending on their switch pattern, which is measured by the interconnectivity to the other states in the MM state map. One shows a more organized and more straightforward switch pattern while the other has more complexity in terms of the switches of the states. Through the observation in the IWBC series, the transition between these two groups of states likely occurs below medium peaks. Similarly, through observing the criticality dynamics map, a group of organized brain states is likely on the right-most tail, and hub-like state nodes are likely on the right above the criticality.

In general, the few gigantic avalanche peaks (usually the first and second tallest peaks) are most likely to remain consistent and organized no matter how high the value of k is.

CHAPTER 5

CONCLUSIONS

Many researchers have employed BOLD fMRI in brain study, in that, in comparison to other techniques, fMRI offers both high spatial and temporal resolutions. The advance in technology then gives rise to a large-scale volumetric dataset for brain analysis. Recently, studies based on the avalanches with fMRI has been of high interest. This work then stresses the study of the novel IWBC avalanche via CAP analysis.

5.1 State decomposition and the point process technique

In this work, on the one hand, the global fMRI signal measure used IWBC calculation. The resultant IWBC series was then employed as the temporal marker to investigate the brain spatial CAPs. On the other hand, an initial voxel-wise brain activity detection was done by thresholding the fMRI volume over the time course. The spatial CAPs characterization was then performed on the pertaining data after thresholding. As a result, instead of representing the information by fMRI volume, the instantaneous brain spatial activity was represented by a vector (ISFs) that included the total activity calculation at particular brain ROIs. By grouping these temporal vectors via the k-means clustering algorithm, we then approached k spatial CAPs in the IWBC series. From a perspective of whole-brain activity decomposition, the k spatial CAPs can express the k decomposed brain states.

Additionally, this work introduced the assessment of the point process technique, which is inspired by the avalanche detection approach in [21]. Unlike clustering over the entire series, the clustering was based solely on the few brief avalanche peaks of high brain organization. Then an evaluation was performed by comparing the generated spatial CAPs from two types of CAP methods. Also, the

similarity measure from the comparison was conducted to study CAP behaviors at the few IWBC avalanche peaks.

Through the observation of spatial CAP maps, it can be concluded that the IWBC calculation generally expresses the activeness of brain states. High IWBC values generally correspond to active spatial CAPs. Another significant aspect is that underlying either a rudimentary or finer detailed anatomical brain mapping, the spatial CAPs tend to have an overall organized arrangement. The spatial map components, such as the major brain lobes or Brodmann areas, are likely to activate and deactivate synchronously with IWBC value. However, investigating the spatial CAPs at a few medium and tall avalanche peaks, some Brodmann areas might show irregular activation patterns. These Brodmann areas included in parts of the cingulate cortex (PCC and ACC), prefrontal cortex (PFC), visual cortex (V2, V3, V4, V5), and Wernicke's area, might dominate the local activation or immediately deactivate when the brain state is increasingly active. Likewise, underlying the RSNs mapping, this work identified that the spatial CAP might behave in a significantly different pattern before and after the IWBC avalanche peaks. Furthermore, assessing the application of the point process technique, the few gigantic avalanche peaks seem to condense more information regarding brain activity, which indicates that the brain may tend to coactivate at these discrete "extreme events." Overall, these observed irregularities and information compactness at avalanche peaks suggest that further researching on avalanche peaks would be worthwhile to understand the brain better.

5.2 Temporal dynamics identification

The second aim of this work is to explore the temporal dynamics of spatial CAPs (or equivalently, brain states). A k-state MM model was introduced with the input received from the labeled brain state sequence. The MM then performed probabilistic analysis and output the transition matrix that incorporated the transition probabilities among states. Thus, the switches and consistency of brain states can be analyzed.

Through a probabilistic interpretation of the state transition in the IWBC series, the overall brain states tend to switch to the same states. Notably, the brain states at very tiny and gigantic avalanche peaks have shown a significantly high consistency. Additionally, the directed graph analysis was also performed to explore the switch pattern. Interconnectivity of the brain states (vertices) in the MM state map (directed graph) then measures the complexity of the switch pattern. Consequently, the presence of a graph division can then be identified. One smaller subgraph (group of states) displays a more organized and straightforward switch pattern, while the other group of states shows more complexity. The few gigantic avalanche peaks, in particular, are most likely to remain a consistent and organized state switch pattern.

In conclusion, this work applies a specific whole-brain correlation analysis for avalanche detection. The CAP analysis is then provided as a particular aspect to study brain behaviors at avalanches. Through inspecting the spatial CAP maps, the medium and tall avalanche peaks tend to introduce some irregular patterns, as described in 5.1. Additionally, further analysis of CAP dynamics then shows the significantly consistent and organized state switch pattern at the few gigantic avalanche peaks outside the criticality [21]. It would be very intriguing and meaningful to continue investigating the brain behaviors at avalanches. The next section will highlight some future directions for the current work.

5.3 Limitations and Future directions

First, this final section looks back at the limitations in this work, including the data and methods. Then, we speculate on some future directions that could be worth investigating further to expand upon the current work.

In this work, either in the assessment of the point process technique or state decomposition analysis, IWBC avalanche peaks have shown to play an essential role in studying brain activity, and thus, require further studies. However, an issue that is not addressed in this study is the nature of avalanches. Some researchers have raised that these cascades of the high global correlation may result from the subject's

head motions or deep breathing. Therefore, a recommended future direction would extend this work to the fMRI data with and without such physiological noises and artifacts, which may assist in identifying the neural origins of the avalanches. Also, some denoising techniques and tools, such as the Independent Component Analysis (ICA) provided by *MELODIC* packages of the FMRIB Software Library (FSL), can help to permit manual identification of these noises within the time series [3], [85], [97].

Another limitation lies in the IWBC calculation and brain activity detection. In our IWBC calculation, all voxels throughout the brain contribute to the instantaneous global correlation value. However, brain activity detection simply applies a threshold value to all brain voxels. Therefore, the Z-scores thresholding at each point in time can cause a lack of BOLD information of the significant voxels. This then explains the reason why the relatively high IWBC value can link to a quiet spatial CAP, in that a few voxels are having significantly high BOLD signal values though the total activity is low. Thus, instead of IWBC calculation, it would be intriguing to use different global fMRI signal statistical measures, such as the calculation of spatial maxima (described in chapter 2 as *Max Size* cluster), to analyze CAP. Then, an assessment can be performed based on variants of defining the global fMRI signal. Also, in terms of the fMRI data, future work can extend to compare the brain behaviors at avalanches between health control and patients with brain disease. It would be a fruitful area to study brain pathologies.

More broadly, a practical future direction can be applying multiple unsupervised learning techniques and preprocessing algorithms to approach brain CAP. Apart from the k-means clustering method, other algorithms, such as minimum spanning tree (MST) [98] and self-organizing map (SOM) [99], are particularly intriguing for further investigation. Given the MST algorithm as an example, a voxel-wise brain topological map can be built based on the temporal correlation among voxels. The edge distances, for instance, can measure the temporal correlation values. Thus, the resultant MST demonstrates the functional brain connectivity in a voxel dimension. Once the MST has obtained, many aspects of further studies can be carried out. One particularly thought-provoking aspect might be applying the MST result

to the data preprocessing before clustering. When considering the voxel-wise clustering method, one approach to obtain a less complicated clustering result is through using a smaller dataset. Then, by taking account of the voxel-wise connectivity, the MST may help to reduce the size of the dataset and improve the quality of the clustering result.

Finally, delineating the voxel-wise spatial movement of avalanches can be a future direction. This popular potential is proposed by [29] as well. In this work, we have observed that the spatial CAP sometimes behaves differently before and after avalanche peaks, which suggests a notable occurrence of spatial propagation during avalanches. However, the spatial CAP in this work is defined by the total activity calculation at some selected brain ROIs, and accordingly, lacks the detailed identification of the spatial movement. Therefore, it would be more convincing to identify the voxel-wise spatial movement as presented in [29], where the white matter trajectories at avalanches are demonstrated. Also, it would be interesting to identify the spatial movement between criticality and avalanche in the critical brain system, which may assist in explaining brain behaviors.

In conclusion, this work generally analyzes brain CAPs via the novel tool IWBC. The CAPs at few avalanche peaks are notably consistent, and these IWBC time frames contain more information about brain activity. This agrees with the recent studies that time-varying information in fMRI tends to be condensed into brief intervals. Avalanches, popularized by Tagliazucchi [21], draw attention to investigating the “dynamic” information about the brain. DFC, for instance, analyzes the time-varying information about FC. Also, applying the sliding window to analyze the time-varying correlation pattern throughout the brain would be interesting. Overall, the aim of this thesis has been to extend the work of Tagliazucchi [21] and Bell [29], whose contributions to the areas of avalanche investigation and observation of CAPs throughout the brain, respectively, provided the impetus for the current research. This work’s primary focus on CAP analysis has yielded notable results regarding avalanches. As such, there is considerable potential for this line of analysis to be coupled with future work to explore avalanches more thoroughly.

REFERENCES

[1] J. M. Beggs, "The criticality hypothesis: how local cortical networks might optimize information processing," *Philosophical Transactions of the Royal Society A: Mathematical, Physical and Engineering Sciences,* vol. 366, no. 1864, pp. 329-343, 2008.

[2] M. D. Greicius, B. Krasnow, A. L. Reiss and V. Menon, "Functional connectivity in the resting brain: a network analysis of the default mode hypothesis," *Proceedings of the National Academy of Sciences,* vol. 100, no. 1, pp. 253-258, 2003.

[3] C. F. Beckmann and S. M. Smith, "Probabilistic independent component analysis for functional magnetic resonance imaging," *IEEE transactions on medical imaging,* vol. 23, no. 2, pp. 137-152, 2004.

[4] C. F. Beckmann, M. DeLuca, J. T. Devlin and S. M. Smith, "Investigations into resting-state connectivity using independent component analysis," *Philosophical Transactions of the Royal Society B: Biological Sciences,* vol. 360, no. 1457, pp. 1001-1013, 2005.

[5] M. D. Fox and M. E. Raichle, "Spontaneous fluctuations in brain activity observed with functional magnetic resonance imaging," *Nature reviews neuroscience,* vol. 8, no. 9, pp. 700-711, 2007.

[6] M. E. Raichle, "The brains dark energy," *Science,* vol. 314, no. 5803, pp. 1249-1250, 2006.

[7] S. M. Smith, P. T. Fox, K. L. Miller, D. C. Glahn, P. M. Fox, C. E. Mackay, N. Filippini , K. E. Watkins, R. Toro, A. R. Laird and C. F. Beckmann, "Correspondence of the brain's functional architecture during activation and rest," *Proceedings of the National Academy of Sciences,* vol. 106, no. 31, pp. 13040-13045, 2009.

[8] J. M. Beggs and D. Plenz, "Neuronal avalanches in neocortical circuits," *Journal of neuroscience,* vol. 23, no. 35, pp. 11167-11177, 2003.

[9] T. Petermann, M. Lebedev, M. Nicolelis and D. Plenz, "Neuronal avalanches in vivo," *In Society for Neuroscience Abstracts,* vol. 531, pp. 101-110, 2006.

[10] M. Paczuski, S. Maslov and P. Bak, "Avalanche dynamics in evolution, growth, and depinning models," *Physical Review E,* vol. 53, no. 1, p. 414, 1996.

[11] T. E. Harris, *The theory of branching process*, Santa Monica, CA: RAND Corporation, 1964.

[12] M. Benayoun, M. Kohrman, J. Cowan and W. van Drongelen, "EEG, temporal correlations, and avalanches," *Journal of Clinical Neurophysiology,* vol. 27, no. 6, pp. 458-464, 2010.

[13] H. J. Jensen, *Self-organized criticality: emergent complex behavior in physical and biological systems*, vol. 10, Cambridge university press, 1998.

[14] D. Plenz and T. C. Thiagarajan, "The organizing principles of neuronal avalanches: cell assemblies in the cortex?," *Trends in neurosciences,* vol. 30, no. 3, pp. 101-110, 2007.

[15] R. L. Buckner, J. R. Andrews-Hanna and D. L. Schacter, "The brain's default network: Anatomy, function, and relevance to disease," *Annals of the New York Academy of Sciences,* vol. 1124, pp. 1-38, 2008.

[16] M. D. Greicius, G. Srivastava, A. L. Reiss and V. Menon, "Default-mode network activity distinguishes Alzheimer's disease from healthy aging: evidence from functional MRI," *Proceedings of the National Academy of Sciences,* vol. 101, no. 13, pp. 4637-4642, 2004.

[17] S. A. Rombouts, F. Barkhof, R. Goekoop, C. J. Stam and P. Scheltens, "Altered resting state networks in mild cognitive impairment and mild Alzheimer's disease: an fMRI study," *Human brain mapping,* vol. 26, no. 4, pp. 231-239, 2005.

[18] K. A. Celone et al., "Alterations in memory networks in mild cognitive impairment and Alzheimer's disease: an independent component analysis," *Journal of Neuroscience,* vol. 26, no. 40, pp. 10222-10231, 2006.

[19] L. Wang et al., "Changes in hippocampal connectivity in the early stages of Alzheimer's disease: evidence from resting state fMRI," *Neuroimage,* vol. 31, no. 2, pp. 496-504, 2006.

[20] C. Sorg et al., "Selective changes of resting-state networks in individuals at risk for Alzheimer's disease," *Proceedings of the National Academy of Sciences,* vol. 104, no. 47, pp. 18760-18765, 2007.

[21] E. Tagliazucchi, P. Balenzuela, D. Fraiman and D. R. Chialvo, "Criticality in Large-Scale Brain fMRI Dynamics Unveiled by a Novel Point Process Analysis," *Frontiers in Physiology,* vol. 3, p. 15, 2012.

[22] E. Tagliazucchi, M. Siniatchkin, H. Laufs and D. R. Chialvo, "The Voxel-Wise Functional Connectome Can Be Efficiently Derived from Co-activations in a Sparse Spatio-Temporal Point-Process," *Frontiers in Neuroscience,* vol. 10, p. 381, 2016.

[23] X. Liu and J. H. Duyn, "Time-varying functional network information extracted from brief instances of spontaneous brain activity," *Proceedings of the National Academy of Sciences,* vol. 110, no. 11, pp. 4392-4397, 2013.

[24] X. Liu, C. Chang and J. H. Duyn, "Decomposition of spontaneous brain activity into distinct fMRI co-activation patterns," *Frontiers in systems neuroscience,* vol. 7, p. 101, 2013.

[25] X. Liu and J. H. Duyn, "Resting-state fMRI signal anti-correlation exists in absence of global signal regression," in *proceedings of 21st ISMRM Annual Meeting*, Salt Lake City, 2013.

[26] X. Liu, N. Zhang, C. Chang and J. H. Duyn, "Co-activation patterns in resting-state fMRI signals," *NeuroImage,* vol. 180, pp. 485-494, 2018.

[27] A. Nalci, B. D. Rao and T. T. Liu, "Global signal regression acts as a temporal downweighting process in resting-state fMRI," *Neuroimage,* vol. 152, pp. 602-618., 2017.

[28] H. He and T. T. Liu, "A geometric view of global signal confounds in resting-state functional MRI," *Neuroimage,* vol. 59, no. 3, pp. 2339-2348., 2012.

[29] C. S. Bell, "Seed-Based Correlation Analysis and Instantaneous Global Correlation Analysis for Resting State FMRI," PhD dissertation, School of Engineering, Vanderbilt University, Nashville, 2018.

[30] H. Maltby, "Brilliant," [Online]. Available: https://brilliant.org/wiki/markov-chains/.

[31] S. Ogawa, T. M. Lee, A. R. Kay and D. W. Tank, "Brain magnetic resonance imaging with contrast dependent on blood oxygenation," *Proceedings of the National Academy of Sciences,* vol. 87, no. 24, pp. 9868-9872, 1990.

[32] D. W. McRobbie, E. A. Moore, M. J. Graves and M. R. Prince, *MRI from Picture to Proton*, Cambridge, UK: Cambridge university press, 2017.

[33] S. A. Huettel, A. W. Song and G. McCarthy, *Functional magnetic resonance imaging*, vol. 1, Sunderland, MA: Sinauer Associates, 2004.

[34] Wikipedia contributors, "Larmor precession," [Online]. Available: https://en.wikipedia.org/w/index.php?title=Larmor_precession&oldid=953698870.

[35] M. G. Bingabr, "Physics of Magnetic Resonance," [Online]. Available: https://slideplayer.com/slide/5923045/.

[36] A. Filler, "Spin Echo Diagram," [Online]. Available: https://en.wikipedia.org/wiki/File:Spin_Echo_Diagram.jpg.

[37] M. Hammer, "MRI Physics: Pulse Sequences," [Online]. Available: http://xrayphysics.com/sequences.html.

[38] A. D. Elster, "Gradient Coils," [Online]. Available: https://mriquestions.com/gradient-coils.html.

[39] K. Barbé, W. Van Moer and G. Nagels, "Fractional-order time series models for extracting the haemodynamic response from functional magnetic resonance imaging data," *IEEE transactions on biomedical engineering,* vol. 59, no. 8, pp. 2264-2272, 2012.

[40] M. H. Sundman, E. E. Hall and N. K. Chen, "Examining the relationship between head trauma and neurodegenerative disease: A review of epidemiology, pathology and neuroimaging techniques," *Journal of Alzheimer's disease & Parkinsonism,* vol. 4, 2014.

[41] M. J. Lowe, "The emergence of doing "nothing" as a viable paradigm design," *Neuroimage,* vol. 62, no. 2, pp. 1146-1151, 2012.

[42] M. H. Lee, C. D. Smyser and J. S. Shimony, "Resting-state fMRI: a review of methods and clinical applications," *American Journal of neuroradiology,* vol. 34, no. 10, pp. 1866-1872, 2013.

[43] D. Mantini, M. G. Perrucci, C. Del Gratta, G. L. Romani and M. Corbetta, "Electrophysiological signatures of resting state networks in the human brain," *Proceedings of the National Academy of Sciences,* vol. 104, no. 32, pp. 13170-13175, 2007.

[44] M. B. C. F. D. S. De Luca, C. F. Beckmann, N. De Stefano, P. M. Matthews and S. M. Smith, "fMRI resting state networks define distinct modes of long-distance interactions in the human brain," *Neuroimage,* vol. 29, no. 4, pp. 1359-1367, 2006.

[45] W. W. Seeley et al., "Dissociable intrinsic connectivity networks for salience processing and executive control," *Journal of Neuroscience,* vol. 27, no. 9, pp. 2349-2356, 2007.

[46] *Neurological disorders: public health challenges*, Geneva: World Health Organization, 2006.

[47] D. J. Thurman, C. M. Branche and J. E. Sniezek, " The epidemiology of sports-related traumatic brain injuries in the United States: recent developments," *The Journal of head trauma rehabilitation,* vol. 13, no. 2, pp. 1-8, 1998.

[48] S. Shively, A. I. Scher, D. P. Perl and R. Diaz-Arrastia, "Dementia resulting from traumatic brain injury: what is the pathology?," *Archives of neurology,* vol. 69, no. 10, pp. 1245-1251, 2012.

[49] S. Jafari, M. Etminan, F. Aminzadeh and A. Samii, "Head injury and risk of Parkinson disease: a systematic review and meta-analysis," *Movement disorders,* vol. 28, no. 9, pp. 1222-1229, 2013.

[50] J. D. Power et al., "Functional network organization of the human brain," *Neuron,* vol. 72, no. 4, pp. 665-678, 2011.

[51] X. J. Chai, A. N. Castañón, D. Öngür and S. Whitfield-Gabrieli, "Anticorrelations in resting state networks without global signal regression," *Neuroimage,* vol. 59, no. 2, pp. 1420-1428, 2012.

[52] Z. Zhang et al., "Resting-state brain organization revealed by functional covariance networks," *PLoS One,* vol. 6, no. 12, 2011.

[53] G. Doucet et al., "Brain activity at rest: a multiscale hierarchical functional organization," *Journal of neurophysiology,* vol. 105, no. 6, pp. 2753-2763, 2011.

[54] Y. Golland, P. Golland, S. Bentin and R. Malach, "Data-driven clustering reveals a fundamental subdivision of the human cortex into two global systems," *Neuropsychologia,* vol. 46, no. 2, pp. 540-553, 2008.

[55] R. Me and M. A. Mintun, "Brain work and brain imaging," *Annu Rev Neurosci,* vol. 29, pp. 449-76, 2006.

[56] M. D. Greicius et al., "Persistent default-mode network connectivity during light sedation," *Human brain mapping,* vol. 29, no. 7, pp. 839-847, 2008.

[57] J. S. Damoiseaux et al., "Consistent resting-state networks across healthy subjects," *Proceedings of the national academy of sciences,* vol. 103, no. 37, pp. 13848-13853, 2006.

[58] B. B. Biswal et al., "Toward discovery science of human brain function," *Proceedings of the National Academy of Sciences,* vol. 107, no. 10, pp. 4734-4739, 2010.

[59] Z. Shehzad et al., "The resting brain: unconstrained yet reliable," *Cerebral cortex,* vol. 19, no. 10, pp. 2209-2229, 2009.

[60] C. Chang and G. H. Glover, "Time–frequency dynamics of resting-state brain connectivity measured with fMRI," *Neuroimage,* vol. 50, no. 1, pp. 81-98, 2010.

[61] E. A. Allen, E. Damaraju, S. M. Plis, E. B. Erhardt, T. Eichele and V. D. Calhoun, "Tracking whole-brain connectivity dynamics in the resting state," *Cerebral cortex,* vol. 24, no. 3, pp. 663-676, 2014.

[62] R. M. Hutchison, T. Womelsdorf, J. S. Gati, S. Everling and R. S. Menon, "Resting-state networks show dynamic functional connectivity in awake humans and anesthetized macaques," *Human brain mapping,* vol. 34, no. 9, pp. 2154-2177, 2013.

[63] Z. Shi, B. P. Rogers, L. M. Chen, V. L. Morgan, A. Mishra, D. M. Wilkes and J. C. Gore, "Realistic models of apparent dynamic changes in resting-state connectivity in somatosensory cortex," *Human brain mapping,* vol. 37, no. 11, pp. 3897-3910, 2016.

[64] B. Biswal, F. Zerrin Yetkin, V. M. Haughton and J. S. Hyde, "Functional connectivity in the motor cortex of resting human brain using echo-planar MRI," *Magnetic resonance in medicine,* vol. 34, no. 4, pp. 537-541, 1995.

[65] M. E. Raichle, A. M. MacLeod, A. Z. Snyder, W. J. Powers, D. A. Gusnard and G. L. Shulman, "A default mode of brain function," *Proceedings of the National Academy of Sciences,* vol. 98, no. 2, pp. 676-682, 2001.

[66] M. D. Fox, M. Corbetta, A. Z. Snyder, J. L. Vincent and M. E. Raichle, "Spontaneous neuronal activity distinguishes human dorsal and ventral attention systems," *Proceedings of the National Academy of Sciences,* vol. 103, no. 26, pp. 10046-10051, 2006.

[67] J. L. Vincent, I. Kahn, A. Z. Snyder, M. E. Raichle and R. L. Buckner, "Evidence for a frontoparietal control system revealed by intrinsic functional connectivity," *Journal of neurophysiology,* vol. 100, no. 6, pp. 3328-3342, 2008.

[68] E. Bullmore and O. Sporns, "Complex brain networks: graph theoretical analysis of structural and functional systems," *Nature reviews neuroscience,* vol. 10, no. 3, pp. 186-198, 2009.

[69] R. Salvador, J. Suckling, C. Schwarzbauer and E. Bullmore, "Undirected graphs of frequency-dependent functional connectivity in whole brain networks," *Philosophical Transactions of the Royal Society B: Biological Sciences,* vol. 360, no. 1457, pp. 937-946, 2005.

[70] M. Van Den Heuvel, R. Mandl and H. H. Pol, "Normalized cut group clustering of resting-state FMRI data," *PloS one,* vol. 3, no. 4, 2008.

[71] R. Salvador, J. Suckling, M. R. Coleman, J. D. Pickard, D. Menon and E. D. Bullmore, "Neurophysiological architecture of functional magnetic resonance images of human brain," *Cerebral cortex,* vol. 15, no. 9, pp. 1332-1342, 2005.

[72] D. Cordes, V. Haughton, J. D. Carew, K. Arfanakis and K. Maravilla, "Hierarchical clustering to measure connectivity in fMRI resting-state data," *Magnetic resonance imaging,* vol. 20, no. 4, pp. 305-317, 2002.

[73] M. H. Lee, "Clustering of resting state networks," *PloS one,* vol. 7, no. 7, 2012.

[74] J. Taylor, *Neural Network Applications*, London: Springer London, 1992.

[75] F. Pereira, T. Mitchell and M. Botvinick, "Machine learning classifiers and fMRI: a tutorial overview," *Neuroimage,* vol. 45, no. 1, pp. S199-S209, 2009.

[76] N. U. Dosenbach et al., "Prediction of individual brain maturity using fMRI," *Science,* vol. 329, no. 5997, pp. 1358-1361, 2010.

[77] D. R. Chialvo, "Emergent complex neural dynamics," *Nature physics,* vol. 6, no. 10, pp. 744-750, 2010.

[78] L. De Arcangelis and H. J. Herrmann, "Activity-dependent neuronal model on complex networks," *Frontiers in physiology,* vol. 3, p. 62, 2012.

[79] D. R. Chialvo, "Critical brain networks," *Physica A: Statistical Mechanics and its Applications,* vol. 340, no. 4, pp. 756-765, 2004.

[80] J. M. Beggs and D. Plenz, "Neuronal avalanches are diverse and precise activity patterns that are stable for many hours in cortical slice cultures," *Journal of neuroscience,* vol. 24, no. 22, pp. 5216-5229, 2004.

[81] N. M. Khairi, D. M. Wilkes and Z. Ding, "Modified Principal Component Analysis in sliding windowed fMRI data," in *IEEE 2019 SoutheastCon*, 2019.

[82] P. Bak, C. Tang and K. Wiesenfeld, "Self-organized criticality: An explanation of the 1/f noise," *Physical review letters,* vol. 59, no. 4, p. 381, 1987.

[83] S. Zapperi, K. B. Lauritsen and H. E. Stanley, "Self-organized branching processes: mean-field theory for avalanches," *Physical review letters,* vol. 75, no. 22, pp. 4071-4074, 1995.

[84] A. Levina, J. M. Herrmann and M. Denker, "Critical branching processes in neural networks," in *PAMM: Proceedings in Applied Mathematics and Mechanics*, Berlin, 2007.

[85] S. Wiegert, "Neuronal avalanches in the human brain: an fMRI study," Diploma thesis, Humboldt-Universität zu Berlin, Berlin, 2015.

[86] M. Glasser et al., "The minimal preprocessing pipelines for the Human Connectome Project," *NeuroImage,* vol. 80, pp. 105-124, 2013.

[87] M. Brett, I. S. Johnsrude and A. M. Owen, "The problem of functional localization in the human brain," *Nature reviews neuroscience,* vol. 3, no. 3, pp. 243-249, 2002.

[88] R. Turner, “Signal sources in bold contrast fMRI,” in *Optical Imaging of Brain Function and Metabolism 2*, vol. 413, Springer, Boston, MA, 1997, pp. 19-25.

[89] M. J. Lowe and D. P. Russell, “Treatment of baseline drifts in fMRI time series analysis,” *Journal of computer assisted tomography,* vol. 23, no. 3, pp. 463-473, 1999.

[90] Wikipedia contributors, “Lobes of the brain,” [Online]. Available: https://en.wikipedia.org/w/index.php?title=Lobes_of_the_brain&oldid=955734515.

[91] K. Brodmann, *Vergleichende Lokalisationslehre der Großhirnrinde : in ihren Prinzipien dargestellt auf Grund des Zellenbaues*, Barth, 1909.

[92] Wikipedia contributors, “Brodmann area,” [Online]. Available: https://en.wikipedia.org/w/index.php?title=Brodmann_area&oldid=955689009.

[93] V. Beliveau et al., “A high-resolution in vivo atlas of the human brain's serotonin system,” *Journal of Neuroscience,* vol. 37, no. 1, pp. 120-128, 2017.

[94] Wikipedia contributors, “Brain atlas,” [Online]. Available: https://en.wikipedia.org/w/index.php?title=Brain_atlas&oldid=919327894.

[95] G. E. Doucet, W. H. Lee and S. Frangou, “Evaluation of the spatial variability in the major resting-state networks across human brain functional atlases,” *Human Brain Mapping,* vol. 40, no. 15, pp. 4577-4587, 2019.

[96] K. Wagstaff, C. Cardie, S. Rogers and S. Schrödl, “Constrained k-means clustering with background knowledge,” in *Icml*, 2001.

[97] S. M. Smith et al., “Advances in functional and structural MR image analysis and implementation as FSL,” *Neuroimage,* vol. 23, no. S1, pp. 208-219, 2004.

[98] B. M. Moret and H. D. Shapiro, “An Empirical Assessment of Algorithms for Constructing a Minimum Spanning Tree,” in *Computational Support for Discrete Mathematics*, vol. 15, pp. 99-117.

[99] T. Kohonen, E. Oja, O. Simula, A. Visa and J. Kangas, “Engineering applications of the self-organizing map,” in *Proceedings of the IEEE*, 1996.